RSC Advances

ROYAL SOCIETY OF CHEMISTRY

www.rsc.org/advances

Phosphate removal by a nano-biosorbent from the synthetic and real (*Persian Gulf*) water

M. Arshadi[*1], J. Etemad Gholtash[2], H. Zandi[3], S. Foroughifard[4]

[1]Department of Chemistry, Shiraz Branch, Islamic Azad University, P.O. Box 71955-149 Shiraz, Fars, Iran

[2]Department of Chemistry, Firozabad Branch, Islamic Azad University, Firozabad, Fars, Iran

[3]Department of Chemistry, Yadegar-e-Imam Khomeini (RAH), Shahre-rey Branch, Islamic Azad University, Tehran, Iran

[4]Department of Fishery, University of Guilan, P.O. Box 1144, sowmesara, Iran

Abstract

The performance of ostrich bone waste-supported nanoscale zero valent iron (OBW-HNO_3-NZVI) adsorbent for phosphate removal from the synthetic and real waters have been evaluated, and the materials were studied by X-ray diffraction (XRD), surface area measurements (BET), transmission electron microscopy (TEM), chemical analysis (CHN), Fourier transform infrared (FTIR), inductively coupled plasma atomic emission spectroscopy (ICP-AES) and point of zero (pH_{PZC}). Iran is the world's third largest breeder and producer of ostrich meat, after South Africa and China. The combination of ZVI particles on the surface of modified ostrich bone waste can help to overcome the disadvantage of ultra-fine powders which may have strong tendency to agglomerate into larger particles, resulting in an adverse effect on both effective surface area and catalyst performance. Good dispersion of NZVI particles (ca. 5–45 nm) on the bone waste was observed. The contact time to attain equilibrium for maximum adsorption of phosphate (99%) was found to be 5 min. The adsorption kinetics of phosphate (P) has been evaluated in terms of pseudo-first- and -second-order kinetics, and the Freundlich, Langmuir and Langmuir-Freundlich isotherm models have also been used to the equilibrium adsorption results. The adsorption process was spontaneous and endothermic in nature and followed pseudo-second-order kinetic model.XRD analysis showed the appearance of $Fe_3(PO_4)_2.8H_2O$ (vivianite) on the OBW-HNO_3-NZVI surface after adsorption of P from aqueous media. The immobilized NZVI indicated high reusability because of its high removal capacity after 12th adsorption–desorption cycles. The developed adsorbent could also be used to remove the P ions from the real sample (*Persian Gulf* water). The high removal capacity of P ions from the real water and the high levels of reusability confirmed the versatility of this nanobiomaterial based on ostrich bone waste.

Keywords: Ostrich bone waste, phosphate, Adsorption, NZVI, *Persian Gulf* water**.**

1. Introduction

[*] To whom correspondence should be addressed. Tel.: +989361528179.
. E-mail Address: m-arshadi@ch.iut.ac.ir, mohammadarshadi@yahoo.com(M. Arshadi)

The liberation and accumulation of phosphate ions into the immobile water bodies such as lakes and estuaries has taken appreciable consideration worldwide in recent years due to the eutrophication [1]. Phosphates are utilized for military applications, sodium lamps, in steel production, special glasses in (incendiary bombs, smoke screenings etc.), and in other implementations, such as toothpaste, detergents, pyrotechnics, and pesticides. Phosphorus is a vital element in agriculture; it is a limited resource and undeniable evidence confirms that current global reserves of P could be used up in 100 years [1]. Excess phosphate and run-offs from agricultural production can cause serious water contamination. In general, phosphorus is present in different forms of phosphate in aqueous media, such as organic orthophosphate, phosphate, polyphosphate, and metaphosphates, where orthophosphate is the most predominant species of phosphate in treated municipal and industrial wastewater and has three acid ionization constant (pKa1 = 2.1, pK_{a2} = 7.2, and pK_{a3} = 12.3), showing that at above pH 7.2, the primary species that presents in the aqueous phase is HPO^{-2}_4 [2]. Raw municipal wastewater may contain phosphorus from 4 to 15 mg P/L [3]; however industrial wastewater, i.e. metal coating processes and, detergent manufacturing may include phosphate levels in excess of 10 mg P/L [4]. When high phosphate concentrations remain in water, algae and other aquatic plant life will flourish eventually causing reduced dissolved oxygen levels and eliminating photosynthesis and productivity in the water [5]. The increase of macrophytes and phytoplankton is motivated predominantly by phosphorus and nitrogen. The growth of rooted aquatic macrophytes will interfere with navigation, aeration, and channel capacity as well the dead macrophytes and phytoplankton will cause of microbial defeat processes [6]. The USEPA has recommended a maximum level of phosphorus in water to be less than 50 mg/L to prevent eutrophication problem and Florida Everglades Forever Act also recommended a new mandate of 10 mg/L of phosphorus in water [8,9].

Various techniques were developed for phosphorus remediation such as electrochemistry [10], membrane bioreactor [11], crystallization [12], biological processes [13] and chemical precipitation [14]. Among the above techniques adsorption processes is considered quite attractive in terms of its low-cost and efficiency of removal of phosphate from dilute solutions [15-17]. Nanoparticles of a variety of shapes, sizes and compositions are changing nowadays the wastewater treatments [18-23]. Preparation and investigation of novel nano materials is important in martial science. Nanostructures can provide an important and feasible platform for catalysis, separation, sensing, and fuel cells [20-25] due to their large specific surface areas and ease with which they can be immobilized onto solid support. They can also be functionalized to increase their affinity towards target compounds in environmental applications. Since the early 1990s, nanoscale zero valent iron (NZVI) has emerged as a new option for the treatment of contaminated soil and groundwater targeting mainly chlorinated organic contaminants (e.g., solvents, pesticides) and inorganic anions, such as phosphate, or metal cations [26]. Moreover, the tendency to form agglomerates using the aforementioned methods could lead to the reduced reactivity and stability of these nanoparticles [26]. NZVI is particularly attractive for sequestration purposes due to its large surface area to weight ratio leading to a greater density of reactive sites. Moreover, the magnetic properties of nano iron facilitate the rapid separation of nano iron from soil and water, via a magnetic field, therefore, it is an effective adsorbent for removing various organic and inorganic contaminants.

Bare NZVI has many advantages such as high reactivity and selectivity, because in bare NZVI every single catalytic entity can act as a single active site [27]. Despite their advantages, in

some cases bare NZVI have not been commercialized because of difficulty encountered when attempting to separate and recovery the bare NZVI from the reaction mixture. Furthermore, some industrial problems such as corrosion and deposition on reactor wall are associated with recover bare NZVI. Disadvantages were minimized if bare NZVI was immobilized onto an insoluble solid supports with excellent chemical and thermal stability and easily accessibility. If support is robust enough to endure the harsh reaction conditions and the NZVI can be used for many times [28].

The aim of the present research is to explain the feasibility of using ostrich bone waste as a low-cost support for NZVI used for phosphate removal from industrial wastewater. Animal slaughtering and the food industry provide meat and bone meal, which are by-products, obtained by the removal of fat from animal carcasses by a process of crushing, cooking and grinding. By-products comprise of nearly 60 to 70% of the slaughtered carcass, of which nearly 40% includes edible and 20% inedible products [29]. To our best knowledge, no attention was paid to examining the adsorption capacity of the materials with biological origin, like ostrich bone treated and activated with NZVI to remove phosphate ions from aqueous solution. In fact, the goal of bone treated is to remove the fat tissues and eliminate the soluble organic contaminants and either modifying the characteristics of adsorbent, as consequence of the immobilization of NZVI.

Ostrich bone waste was selected because Iran is the world's third largest breeder and producer of ostrich meat, after South Africa and China. There are believed to be around 130 Iranian ostrich farms, with local experts insisting that the country possesses the world's best climatic conditions for breeding [30]. Besides setting records, the long-term goal was to create a new cultural appetite for ostrich, which is lower in fat and cholesterol than other meats traditionally popular in Iran.

This work was set out to study how effectively heterogenized NZVI on ostrich bone waste was able to remove phosphate anions from aqueous solution in batch contact experiments. These studies were tailored to study the effect of pH, ionic strength, and coexisting anions on phosphate capture, as well as a determination of the adsorption isotherm and phosphate sorption kinetics in the real water (*Person gulf* water).

2. Experimental section

2.1. Materials

All reagents (A.R.) were purchased from Merck or Aldrich and were used without further purification, except for solvents, which were treated according to standard methods [31].

2.2. Preparation of the modified Ostrich bone waste (OBW)

Ostrich bone waste (OBW) was obtained from a local store and was cut and then its fat and flash were removed cleanly. After separating the fat and their flesh, all remaining ostrich bone waste was put in the oven for 24 hours in 70 ^{o}C, and after drying they were ground and were passed through different sieve size. The fraction of particle between 250 and 400 µm (geometric mean size: 305 µm) was selected. Fresh OBW was washed thoroughly with hot distilled water and was dried at 65 ^{o}C. The sorbent thus obtained was designated pristine ostrich bone waste (OBW). Preliminary studies using OBW treated with acid was carried out in order to optimize the sorption of phosphate ions. The OBW was treated with 0.1 M HNO_3 solution at reflex for 2 h. A typical experimental procedure was as follows: 30 g of OBW were dispensed in 0.5 L of distilled water. Then a certain amount of 0.1 M HNO_3 was added and the suspension

was subjected to mechanical stirring for 2 h on heater. The final material was separated by centrifugation and washes with distilled water. Excess of HNO_3 was removed with distilled water and the material was dried at 50 ^oC. HNO_3 treated OBW was designated as OBW-HNO_3.

2.3. Preparation of the biomaterial-supported NZVI (OBW-HNO_3-NZVI nanobiocomposite)

The NZVI-biomaterial sample was synthesized based on the following procedure: $FeCl_2 \cdot 4H_2O$ was dissolved in a 4/1 (v/v) ethanol/water mixture (72 mL ethanol + 18 mL deionized water), then the OBW-HNO_3 is added to this solution and the mixture is left in an ultrasonic shaker for 25 min in order to disperse the biomaterial grains. Meanwhile, sodium borohydride solution is prepared by dissolving $NaBH_4$ in 100 mL of deionized water. The borohydride solution is then added drop wise to the aqueous Fe(II)–OBW-HNO_3 mixture while stirring continuously on a magnetic stirrer. Black solid particles of NZVI appeared immediately following the addition of the first drop of $NaBH_4$ solution. After the full addition of the borohydride solution, the mixture is left for a further 30 min of stirring and then filtered. Immobilization of NZVI on the OBW-HNO_3 was designated as OBW-HNO_3-NZVI.

2.2. Characterization techniques

The point of zero charge for the adsorbents was determined from the addition method [32]. Nitrogen (99.999%) adsorption experiments were performed at -196ºC using a volumetric apparatus (Quantachrome NOVA automated gas sorption analyzer). All samples were degassed under vaccum at 120ºC for 16h before the adsorption experiments. The specific surface areas of the adsorbents were calculated using the BET method and the pore size was calculated using the Barrett-Joyner-Halenda (BJH) method. FTIR spectra were recorded using a Jasco FT/IR-680 plus spectrophotometer as KBr pellets. XRD studies were carried out using a Philips X'PERT MPD diffractometer. Chemical analyses were carried out by inductively coupled plasma atomic emission spectroscopy (ICP-AES) using a Shimadzu ARL 34000 instrument (spectro-flamed; typically, 30 mg sample was dissolved in 500 µl 40% HF solution, 4mL 1:4 HCl:H_2SO_4 solution and 45 mL H_2O). The image of transmission electron microscopy (TEM) was taken using a Philips 501 micro-scope and a Tecnai F30TEM operating at 300 kV.

2.4. Adsorption measurements

Adsorption experiments were carried out in batch conditions: 0.05 g of modified bone sample was shaken with 50 ml of the phosphate solution, at a concentration of between 0.75 and 1000 mg/L, at a controlled temperature of 25ºC. Each experiment was performed three times and the averaged values were reported that displayed a relative standard deviation lower than 1.4 %. The time required to reach equilibrium conditions was determined by preliminary kinetic measurements. No significant variation in sorption capacity was observed after 24 h of contact. After centrifugation at 3000 r.p.m. for 5 min, the liquid phase was separated and the solute concentration determined using a inductively coupled plasma atomic emission spectroscopy (ICP-AES) using a Shimadzu ARL 34000 instrument.

The amount adsorbed was calculated as:

$$q_e = V.(C_0 - C_e)/m \quad (1)$$

where C_0 and C_e are the initial and equilibrium liquid-phase concentrations (mg/L) of adsorbates; V is the volume of the solution (L); and m is the amount of adsorbent (g). This equation assumed that the change in volume of the bulk liquid phase was negligible as the solute concentration is small and the volume occupied by the adsorbent was also small. The amount of

the phosphate adsorbed on the sample was calculated using a previously determined calibration curve.

3. Results and discussion

3.1. Characterization of pristine and modified ostrich bone waste

Initial experiments indicated that the pristine ostrich bone waste (POBW) has a low potential to adsorb phosphate ions from the wastewater. POBW has more than 80% organic compounds, which 90 to 95% is collagen and proteoglycans, the rest being non-collagenous proteins (matrix proteins), that could cover the inorganic phase of the bone (i.e. hydroxyapatite). So, in this work different processes of pretreatment (acid treatment and NZVI immobilization) are designed to the POBW with the purpose of enhancing the P adsorption potential. The purpose of acid treatment was to remove soluble materials on the POBW surface that might have interfered with its adsorptive properties and also give more active sites and/or by obtaining suitable chemical modification of the available functional groups, creating more active sites which further accelerate immobilization of NZVI.

The implementation of ZVI in nano-scale can improve the reactivity of the material by virtue of the high surface to volume ratio and could also bring about kinetic advantages for adsorption. Another important property of these nanoparticles is their enormous flexibility for in situ and ex situ applications. When the reduction of an aqueous iron salt is done in the presence of a support material, the normally-observed aggregation of iron nanoparticles was reported to decrease. The resulting dispersion of iron nanoparticles offers a higher specific surface area and consequently a higher reactivity of iron to the aqueous stream. In fact, the zero valent iron is not responsible for the removal of P ions while the iron oxide/hydroxide layer on its surface involving in the adsorption of P ions from aqueous solution. The structure of the prepared biomaterials were confirmed by CHN, inductively coupled plasma/atomic emission spectroscopy (ICP–OES), FT-IR, Transmission electron microscopy (TEM), BET (N_2 adsorption–desorption technique), XRD and the point of zero charge (pH_{PZC}).

Inspection of infrared wave numbers (cm^{-1}) of significant valence vibrations of the pristine bone powder before modification, after modification with HNO_3 and NZVI show striking changes, which are collected in Figure 1. The bands at 1625-1665 cm^{-1} are related to organic tissue and water of pristine ostrich bone, while the $–CO_3^{2-}$ band intensities of unmodified bone appear at 1413 and 872 cm^{-1} [33,34]. The pristine bone shows the characteristic absorption bands of symmetric and asymmetric stretching vibration of the CH_2 and CH_3 at around 1455-1470, 2852 and 2922 cm^{-1}, while the presence of a band at 1744 cm^{-1} is related to carbonyl groups. The spectrum in the C-H stretching region shows absorption maxima at 3065 cm^{-1}, which is typical of the C-H stretching vibration of the aromatic rings.

As can be seen from the Figure 1A, the characteristic vibration peaks of O–P–O bonds of calcium phosphate appeared in all the samples as follow: 1165 cm^{-1} (HPO_4^{2-} group, P–O–H in-plane and out-of-plane deformation modes), 1028 and 1100 cm^{-1} (ν_3, P-O asymmetric stretching vibrations), 960 cm^{-1} ($\nu_1$sym, P-O stretch), 603 cm^{-1} (ν_4, P-O stretch), and 560 cm^{-1} (ν_4, P-O stretch and P-O bending) [35,36]. FTIR also bestows an indication of the inorganic phase of the bone, thereby two bands in the region of 1028-1100 cm^{-1} attribute to hydroxyapatite while amorphous calcium phosphate appears a broad single band. However, the characteristic vibration bands of hydroxyapatite are hardly obvious in unmodified bone which could be due to the high

content of organic phase (collagen, fat and organic tissue) which disguises the features of the mineral phase and decreasing the crystallinity of hydroxyapatite. Furthermore, infrared wave numbers of bone powder comprise of some characteristic absorption bands related mainly to the peptide bonds (–CONH–) which known as amide I, amide II, and amide III. The weak intensity of the vibration bands in the range of 1600-1700 cm^{-1}, attribute to C=O stretching vibrations of the amide I and are assigned as a useful indicator of various types of protein secondary structure [35]. Indeed, the α-helical and the λ-sheet structure of the protein giving a maximum peak near 1655 cm^{-1} and 1630 cm^{-1} respectively. The amide I peak of unmodified bone appeared at 1641 cm^{-1}, and 1646 cm^{-1}. The amide II peaks which appeared in the region of 1520-1540 cm^{-1} are assigned to N–H and C–H bending and stretching vibration. The amide III band which falls in the region 1220–1300 cm^{-1}, is attributed to the phase combination of C–N stretching, N–H in plane bending and some contribution from C–C stretching and C=O bending vibrations. Natural proteins and peptides contain a disulphide bond (–S–S–), which appears stretching vibrations near to 510, 525 and 540 cm^{-1} [37,38]. Therefore, the main band at 507 cm^{-1} and the ones at 521 and 530 cm^{-1} with lower intensities were attributed to the disulphide bond of the pristine bone (Figure 1A).

The band intensities 1158, 1096 and 1033 cm^{-1} (vibration bands of hydroxyapatite), 603 cm^{-1} (v_4, P-O stretch) and 561 cm^{-1} (v_4, P-O stretch and P-O bending) increased with modification of bone with HNO_3 (Fig. 1B). The absorption at 3270 cm^{-1} was attributed to water adsorbed on the structure of the bone [39].

The peak shape of the spectrum was changed after modification of OBW-HNO_3 with NZVI (Fig. 1B). The results indicated that the immobilization of NZVI does significant changes in the basic chemical composition of OBW-HNO_3, where the absorption peaks of hydroxyl (a broad absorption peak in 3361 cm^{-1}), 2922 and 2852 cm^{-1} (CH_2 groups of the organic compounds), 1744 cm^{-1} (carbonyl groups), 1662, 1460 and 1433 cm^{-1} (bending vibration of –CH_3), displayed obvious changes. Furthermore, band at 823 and 705 cm^{-1} (OBW-HNO_3-NZVI) was attributed to the iron oxides (Fig. 1C). The band at 634 and 621 cm^{-1} can be assigned to Fe–O stretching vibrations [15,21,23]. The Amide peaks were characteristic of protein bands, and the location of this absorption peaks were changed after immobilization of NZVI, indicating proteins could be carriers for the iron ions during the synthesize and immobilization process. Alternatively, proteins could chelate with iron ions and play an important intermediary role. Furthermore, the band shift of hydroxyapatite vibrations from 1237 to 1220 and 1096 to 997 cm^{-1} are the most significant (Fig. 1B and C). The results in Table 1 also indicated that the hydroxyapatite contents increased as the NZVI was immobilized, suggesting possible binding of iron ions to Ca–O–H and –P–O–H groups of OBW-HNO_3-NZVI.

Fig. 2 shows the surface morphology of the pristine ostrich bone and OBW-HNO_3-NZVI that were analyzed by transmission electron microscope (TEM). The TEM images were taken in backscatter mode to enhance the contrast between the nanoparticles and the support, i.e. the iron appears brighter than the support. The presence of NZVI with higher electron contrast onto the OBW-HNO_3 indicates the immobilization and distribution of nanoiron on the OBW-HNO_3 without aggregation, thereby, nano-particle of iron was rough with a round shape, which was very different from bare Fe(0), where chain-like structures were observed [26]. The coarse and rough morphology of the Fe(0) particles could provide more reactive sites than the smooth morphology. As revealed in Fig. 2B, the NZVI particles (ca. 5–30 nm) immobilized on OBW-HNO_3 were clearly discrete and well dispersed on the modified bone, without aggregation. This confirms why NZVI are commonly immobilized by researchers on support materials such as

resin, starch, clay and zeolite [26] because this decreases the aggregation of NZVI and increases mechanical strength. Thus, OBW-HNO_3 can prevent the NZVI particles from aggregating together. This observation of dispersed iron particles was also in accordance with some published results and provided a good example of dispersion on the surface of modified bone [15,21,23,26].

The chemical compositions of the pristine and modified ostrich bone were determined by CHN and ICP. The ostrich bone contains relevant amounts of animal nutrients like C, Ca, P, K, and Mg (Table 1). In addition, the bone contains a number of elements that are vital to animal in small doses, i.e., micronutrients, but also generally contain small amounts of undesirable heavy metals. CHN analysis of ostrich bone shows the high C content originates from the fat tissues and organic compounds adhesive the framework of pristine ostrich bone. HNO_3 and NZVI treatment removes fat tissues as a change in the color of the extraction liquid can also be visualized, because the extraction liquid is dirty brown. During the modification reactions, the carbon content of pristine bone after HNO_3 and NZVI modification decreased from 79.8 to 18.5 and lower than 5.12 wt.%, respectively, and the calcium and phosphor contents increased. Also, the HNO_3 treatment may induce negative charges via oxidation of organic compounds, which increased the number of active sites of the modified bone (Table 1). The carbon content of OBW-HNO_3-NZVI significantly decreased, which could be due to the removing of the organic compounds by alkali or reaction with NaBH4 and H_2O during the preparation of NZVI. The results in Table 1 also indicated that the calcium phosphorous contents increased as the NZVI was immobilized. It is believed that Fe ions were bound to active sites on the surface of the acid treated OBW, such as -Ca-ONa, and -P-ONa.

The specific surface areas (SSA) of the pristine bone, OBW-HNO_3 and OBW-HNO_3-NZVI were measured using a BET-N_2 surface area analyzer (Table 2). When 15% of NZVI was loaded onto the OBW-HNO_3, a mean specific surface area of 41.4 m^2/g was obtained, which was 11.2 and 2.24 times larger than the pristine bone (3.7 m^2/g) and OBW-HNO_3 (18.42 m^2/g), respectively. As NZVI particles were dispersed onto the surface of OBW-HNO_3, the reactivity was enhanced. The BET surface areas of iron nanoparticles synthesized by other researchers (20–60 m^2/g) being larger than that of OBW-HNO_3-NZVI (41.4 m^2/g), its reaction activity was much lower than that of OBW-HNO_3-NZVI due to more pronounced oxidation and aggregation. Bare NZVI has only limited applications in remediation activities [26], where the surface of NZVI was oxidized easily due to a higher specific surface area and stronger reactivity, that is, supported NZVI was immobilized on the active sites of OBW-HNO_3, which would decrease the oxidation of the NZVI surface. Other possible reasons why immobilized NZVI could exhibit enhanced reactivity include higher density of reactive surface sites and higher reactivity of surface sites.

The X-ray diffraction patterns of pristine and modified ostrich bone are given on Figure 3. Comparison of XRD pattern with JCPDS file confirms the presence of calcium hydroxyapatite (CaHAP) phase [$Ca_{10}(PO_4)_6(OH)_2$], while the broad and intense background were attributed to the organic compounds and also could be due to the small particles and amorphous phase of the hydroxyapatite [33,36]. These results clearly show the poor crystallinity of pristine ostrich bone even after chemical modification, but the XRD patterns of the modified samples showed that calcium phosphate peaks become somewhat higher in intensity after treatment by HNO_3 and NZVI, related to the removal of inward organic compounds from the framework of ostrich bone

and increasing the mineral phase. An increase of the inorganic phase fraction of modified bone sample also appeared and was characterized by an increase of the region intensity at 2θ in 26, 32, 34 and 40 – 50º for OBW-HNO_3 and OBW- HNO_3-NZVI. However, the chemical modification did not create remarkable alters of HAP original crystallinity. The iron nanoparticles consisted mostly of iron, reflections at 2θ of 44.98° (Fig. 3) [26]. This indicated that the iron present on OBW-HNO_3 surface is mainly in its zerovalent state. Iron oxide signals were not detected in the XRD patterns of the freshly prepared samples and even after nine months which demonstrated that the OBW-HNO_3 could be a suitable stabilizer of NZVI. In fact, when the particle size of the NZVI is smaller than 5 nm, the diffractions were significantly broadened and the intensity decreased (Fig. 3) [35].

3.2. Adsorption studies

The effect of pH plays an important role on the active sites of nanobio-adsorbent and the P speciation during the adsorption process. To study the effect of the pH on the removal capacity of OBW-HNO_3-NZVI, experiments were designed at initial concentrations of 70, 250 and 800 mg L^{-1} and pH range between 2.0 and 12.0 (Figure 4A). The modified bone with NZVI indicated higher P adsorption capacity in the acidic values of pH. The results indicated that there was no significant influence of pH (between 2.0 and 7.0) on the adsorption of phosphate by OBW-HNO_3-NZVI while the ionization state of P was pH dependent according to Fig. S1 (pK_{a1} = 2.1, pK_{a2} = 7.2, and pK_{a3} = 12.3). As the initial pH decreased 7.0 to 1.0, the adsorption efficiency gradually increased from 83.5 to more than 89.4 % and decreased sharply at the initial pH range above 8.0 at initial concentration of 70 mg/L (>13.4 %). The lowest P adsorption capacity of OBW-HNO_3-NZVI (13.4 %) was found at an initial pH solution of 12.0, which was caused by the deprotonation of the hydroxyl species on the surface of iron nanoparticles at this solution pH. It is clear from Fig. 4A that the adsorption of P is higher in the acidic pH range of 2-6.0 than in the alkaline range. A plausible explanation was that more oxygen containing functional groups (the dominant active sites of OBW-HNO_3-NZVI are Fe-OH, -P-OH and ≡Ca-O-H species) in the OBW-HNO_3-NZVI became deprotonated and negatively charged as pH increased resulting in lower phosphate anion uptake due to the electrostatic repulsion [40]. At lower pH, the concentration of H^+ ion was high, causing an electrostatic interaction between the acid active sites ion and P anions ($H_2PO^-_4$, Fig. S1). The active sites were closely associated with hydroxyl ions OH^- restricting the approach of P ions, as a result of the repulsive force, and therefore fewer groups are available for the adsorption of P. Therefore, at low pH, the removal efficiency was high. The maximum removal efficiency of 92 % was found for OBW-HNO_3-NZVI at pH 5.0 that was chosen as the optimal pH for the rest of the study.

Zeta potentials of the pristine ostrich bone, OBW-HNO_3 and OBW-HNO_3-NZVI (0.1 mg/ml) were measured in 10^{-3}M NaCl aqueous solution at different pH. The solution pH was adjusted by NaOH or HCl. The pH_{ZPC}, ZPC is defined as the pH at which the total surface charges become zero. All bone samples showed the same behavior. As shown in Fig. 4B, the pH value of point of zero charge (pH_{pzc}) of the pristine ostrich bone was about 7.8. After being modified with HNO_3 and NZVI, the pH_{pzc} shifted to 6.8 and 5.78, respectively, indicating that the immobilization of NZVI onto OBW-HNO_3 was successful and confirm that the surface of the pristine bone was changed after chemical modification. Indeed, pure iron oxides typically have zero point charges (ZPC) in the pH range 7–9 [26]. Therefore, the modified samples yield acidic surface since pH_{pzc} of them were lower than that of the pristine one and this surface acidity was due to the introduction of several oxygen-containing functional groups.

The effect of shaking time (0-30 min) on the adsorption of P (30, 70 and 250 mg L^{-1}) by the OBW-HNO_3-NZVI (0.05 g) at 25°C, in a solution with a pH of 5.0 was shown in Fig. 5A, where the majority of P was removed within the first 2.5 min of contact time with the OBW-HNO_3-NZVI. The black iron nanoscale supported on OBW-HNO_3-NZVI was immediately solubilized (the system turned reddish-brown when there is oxygen in it), that showed that the OBW-HNO_3-NZVI reacted instantly with oxidative matters in the bulk solution. Percentage of maximum adsorption of P ions was 100, 99.8 and 78 % at initial concentration of 30, 70 and 250 mg L^{-}, respectively, after 30 min. Indeed, the fast adsorption during the initial stages is probably due to the high concentration gradient between the adsorbate in solution and that on the adsorbent as there are a high number of vacant sites available during this period, while the obtained plateau after 5 min relates to a slow rate of adsorption which could be due to agglomeration of P ions on the OBW-HNO_3-NZVI active sites. The removal of P ions from solution was complete within 5 min. In order to optimize the adsorption process, the adsorption isotherms for the rest of initial concentrations were examined for a time of 2.0 min.

To determine and interpret the mechanisms of P ions uptake processes over OBW-HNO_3-NZVI and major parameters governing sorption kinetics, kinetic sorption data obtained empirically were fitted to the pseudo-first-order, pseudo-second-order, and intra-particle diffusion models, shown in Table S1. The calculated kinetics parameters for adsorption of P ions on the OBW-HNO_3-NZVI, at different initial concentrations of 30, 70, and 250 mg L^{-1} are tabulated in Table 3. As can be observed, the pseudo-second-order equation appeared to be the better fitting model than those for the other two equations (the correlation coefficient was extremely high for the pseudo-second-order equation of OBW-HNO_3-NZVI; $R^2 > 0.9948$). The value of $q_{e,cal}$ also appeared to be very close to the experimentally observed value of $q_{e,exp}$. The plot of linear form of the pseudo-second-order for the adsorption of P ions is shown in the inset of Fig S2.

The agreement of the experimental result with the pseudo-second-order kinetic model (the pseudo-second order equation was based on the sorption capacity on the solid phase) showed that the removal of P by OBW-HNO_3-NZVI was verified by chemisorption (as the rate-limiting step of the adsorption mechanism and no involvement of a mass transfer in solution) involving valence forces through sharing or exchange electrons between adsorbent and adsorbate. The adsorption of the P on the immobilized NZVI considered to be comprised of two processes with initial adsorption rates of 185.1, 834.0 and 1428 mg (g min)$^{-1}$ for 30, 70, and 250 mg/L, respectively (Table 3), over OBW-HNO_3-NZVI (the adsorption rate was related to the content and type of active adsorption site on the matrix of adsorbent). A further advantage of the pseudo-second-order model was that it predicts the behavior over the whole range of the adsorption process.

The first-order and pseudo-second-order kinetic models could not identify the diffusion mechanism. Thus the kinetic results were then analyzed by using the intra-particle diffusion model. Weber and Moris plot (Table S1; q_t versus $t^{0.5}$) was used to investigate intra-particle diffusion mechanism (Fig. S3). If the intra-particle diffusion was the only rate-controlling step, the plot passed through the origin; if not, the boundary layer diffusion controlled the adsorption to some degree. As seen from Fig. S3, the plots were not linear over the whole time range, implying that more than one process affected the adsorption.

Furthermore, the equilibrium adsorption capacity of P on the favored adsorbent, OBW-HNO_3-NZVI, were studied at various temperatures (15, 25, 60 and 80ºC) at pH = 5.0 (Figure 5B). The increase in the temperature of P solutions from 15 to 80ºC lead to an increase in the

adsorption capacity of the bone samples. This indicated that adsorption of the P on active sites of the OBW-HNO_3-NZVI was endothermic and could be elucidated by availability of more active sites of adsorbent, the enlargement and activation of the adsorbent surface at higher temperatures. This could also be due to the easily mobility of phosphate ions from the bulk solution towards the adsorbent surface and enhanced the accessibility to the adsorbent active sites.

The thermodynamics parameters related to the adsorption of P ions on OBW-HNO_3-NZVI, namely the changes in Gibbs free energy (ΔG^o), enthalpy (ΔH^o) and entropy (ΔS^o) where therefore calculated using the following equation:

$$\Delta G = -RT \ln K \quad (2)$$

where R (8.314 J/mol·K) is the ideal gas constant, T (K) is the temperature and k (L/g) is the distribution coefficient of the adsorbate (q_e/C_e), and the van't Hoff equation:

$$\ln K = \Delta S^o/R - \Delta H^o/RT \quad (3)$$

The $\Delta H°$ and $\Delta S°$ values were calculated from slope and intercept of the linear plot, of lnK vs 1/T as shown in Fig. 6A. The calculated thermodynamic parameters are summarized in Table 4. The results showed a spontaneous and favorable adsorption process over the whole temperature range ($\Delta G < 0$). The standard enthalpy (ΔH) for the adsorption process was positive, thus indicating that the process was endothermic in nature. The necessity of a large amount of heat to remove the P ions from the solution makes the sorption process endothermic. The positive value of ΔS revealed the increased randomness and an increase in the degrees of freedom at the solid-solution interface during the fixation of the P ions on the active site of the adsorbent which indicated the partial dehydration of the P ions before adsorption, thus increasing the spontaneity. This is also supported by the positive value of ΔH, when the positive value of the standard enthalpy change for P ions sorption indicates endodermic nature of adsorption. It could be seen that with a rise in temperature the value of ΔG decreased, which showed that removal processes of P over immobilized NZVI were spontaneous and thermodynamically favorable (Table 4).

The experiment results of the effect of different initial P ion concentrations (0.75–1000 mg L^{-1}) over OBW, OBW-HNO_3 and OBW-HNO_3-NZVI are shown in Fig. S4. The removal of P over the modified bone samples in this study decreased in the order of OBW-HNO_3-NZVI> OBW-HNO_3> OBW. OBW-HNO_3-NZVI was demonstrated to be the most efficient in that more than 91.1% of P was removed after 2.5 min, while only 2.34 and 47 % of P was removed by OBW and OBW-HNO_3, respectively, where initial concentration of P ions was 150 mg L^{-1}. The adsorption was initially fast (i.e., between 0.75 and 250 mg L^{-1}), decreased progressively and finally approached equilibrium. The animal bone waste used in this work was a waste biomaterial and it indicated low efficiency in removal of P, but provided good suspensibility and dispersibility for nanoparticle after modification with HNO_3 and NZVI, when removing P from aqueous solution and it increased the efficiency of OBW-HNO_3-NZVI.

When the initial P concentrations were increased in the presence of OBW-HNO_3-NZVI, the adsorption of the P ions reached to 97.7, 91 and 32.6 % for 30, 110.0 and 1000 mg L^{-1} of phosphate, respectively. However, NZVI had a poor removal efficiency when it was used to remove P with a concentration greater than 100 mg L^{-1}, which may have been caused by the aggregation of NZVI decreasing its specific surface area and reaction activity [41]. Immobilized NZVI on ostrich bone waste was a well dispersed and stable material in aqueous solution. The observed increase of P removal with rising the initial P ions concentration could be related to an

augment in electrostatic interactions (relative to covalent interactions), which involved active sites of progressively lower affinity for P up to saturation point. On the other hand, the higher removal efficiency of OBW-HNO_3-NZVI at low P initial concentration could be attributed to the ratio of mol of phosphate ions to the number accessible active sites on the surface of the adsorbent; that was, the fractional adsorption was determined by the initial concentration. These results suggested that OBW-HNO_3-NZVI could efficiently uptake P from aqueous solution at elevated concentrations.

In order to understand the mechanisms of the adsorption and explain how P ions interacted with the modified bone samples, equilibrium adsorption isotherms could be very important. The experimental adsorption equilibrium results for P on the bioadsorbents were fitted by applying the Langmuir and Freundlich isotherm models (Table S1). There models are commonly utilized to investigate aqueous. These adsorption models (Table S1) give a representation of the adsorption equilibrium between an adsorbate in solution and the active sites of the adsorbent.

where q_e (mg/g) is the specific equilibrium amount of adsorbate, C_e (mg/L) is the equilibrium concentration of adsorbate, q_m is the maximal adsorption capacity and K_L (L/mol) and n are empirical constants that indicate the extent of adsorption and the adsorption effectiveness, respectively. The constant n gives an idea of the grade of heterogeneity in the distribution of energetic centers and is related to the magnitude of the adsorption driving force. High n values therefore indicate a relatively uniform surface, whereas low values mean high adsorption at low solution concentrations. Furthermore, low n values indicate the existence of a high proportion of high-energy active sites.

The Langmuir equation relates the coverage of molecules on a solid surface to the concentration of a medium above the solid surface at a fixed temperature and adsorption is limited to monolayer coverage, and intermolecular forces decrease with the distance from the adsorption surface. The Freundlich model supposes that the adsorption surface is heterogeneous, that interactions between adsorbed molecules can occur, and that multilayer adsorption is possible. The Langmuir and Freundlich adsorption isotherms exhibit an approximately linear relationship for used adsorbent (see Table 5 and Fig. 6B). The results acquired from the studied systems showed that Langmuir isotherm correlated better (R^2=0.96) than Freundlich one.

3.3 Effect of interfering ions on phosphate removal

The widespread existence and interference of anions and alkaline earth metals may affect the removal of P ions from aqueous solution by blocking active adsorption sites or the complexation with of P ions. Therefore, five typical anion species (chloride, nitrate, bicarbonate, sulfate and citrate) at concentrations of 0.01 to 0.1 M were used to evaluate their effect on P adsorption by OBW-HNO_3-NZVI at concentration of 150 mg L^{-1}(Fig. 7). In the absence of any competitive anions, the percent of P removal by OBW-HNO_3-NZVI was as high as 91.2 %. The results depicted in Fig. 7 confirmed that there was only small interference for the P removal by the presence of 0.01 M sodium sulfate, sodium chloride and Sodium citrate. Dissolved sodium bicarbonate competed strongly with phosphate at 0.1 M, suppressing the uptake rate of P from aqueous solution. It can be concluded that OBW-HNO_3-NZVI kept its reactivity in the presence of the used interferences, while $NaHCO_3$> $NaNO_3$> $Na_3C_6H_5O_7$ showed the most suppressing effect on the removal of P ions from aqueous solution. It is believed that metalated adsorbent could bind the anions of higher base strength more strongly than those with lower base strength. Additionally, the presence of salts could support the effect of electric double layer compression

on the surface of OBW-HNO_3-NZVI which blocking active sites on the surfaces, and lead to the liberation of adsorbed P. The decreased of removal capacity of OBW-HNO_3-NZVI towards P ions in the presence of $NaHCO_3$ demonstrated that NZVI prefered to complex with HCO_3^- and decreased affinity of the active sites of OBW-HNO_3-NZVI towards P, which eventually lowered the uptake of P ion from the bulk solution. On the other hand, the initial pH of the solution with 0.1M $NaHCO_3$ was 8.1, at which a large amount of OH^- was present that competed with P ions for the attractive interaction with active sites of immobilized NZVI and obstructed the ligand-exchange mechanism, so decreasing P ions removal from aqueous solution.

3.4. Reusability

To determine the reusability, the used OBW-HNO_3-NZVI was separated by filtration after the first uptake experiments. For extraction of adsorbed phosphate ions different concentrations of NaOH were tested to regenerate active sites on the surface of OBW-HNO_3-NZVI. Finally samples were dried at 80 ◦C under vacuum to be ready for reuse under comparable testing conditions. Increased ionic strength of solution significantly lowered desorption of phosphate ions (Fig. 8A). At a NaOH concentration of 0.1 M, 62.0 % of P were desorbed, while at lower concentrations of NaOH only about 2.0% were released. It was observed that the efficiency of desorption process was generally above 98.6 % at NaOH = 1.0 M, and the adsorption capacity of the regenerated OBW-HNO3-NZVI was almost not affected. No significant loss of activity was observed, confirming that the OBW-HNO_3-NZVI had high stability during the adsorption process even after 12^{th} runs (Fig. 8B). It is believed that OBW-HNO_3, as the host of NZVI, helped to decrease the precipitation of adsorbed P ions on the iron surface (iron hydroxide), therefore, this would have kept the reactive sites (the iron oxide/hydroxide layer) on the immobilized NZVI surface, which results in higher efficiency on removing P after 12^{th} runs. In fact, the zero valent iron is not responsible for the removal of P ions while the iron oxide/hydroxide layer on its surface involving in the adsorption of P ions from aqueous solution.

3.5. Effect of aging time on phosphate uptake

In order to evaluate the effect of aging on the removal capacity of the supported NZVI by modified ostrich bone waste, a set of experiments were designed using freshly prepared OBW-HNO_3-NZVI in addition to samples aged for the periods of 7, 20, 30, 60, 90, 180, 240 and 360 days. The results are shown in Fig. 9 at initial P ion concentrations of 70, 250 and 800 mg L^{-1}. The results indicated that the OBW-HNO_3-NZVI had largely retained its reactivity towards P ions removal from aqueous even after 360 days of preparation (Fig. 9). Additionally, removal of phosphate ions diminished less than 8% due to ageing the OBW-HNO_3-NZVI. The decrease in the removal capacity of the OBW-HNO_3-NZVI aged was related to the concentration, while the decrease was more pronounced for the highest initial concentration (800 mg L^{-1}).

3.6. Real water sample

The suggested adsorbent in this paper was also implemented to remove P from the *Persian Gulf* water as a function of time (Fig. 10). The *Persian Gulf* water gathered from the cost of Bushehr and was filtered using 0.45 µm filter membrane and then they were stored in polyethylene bottles. The concentration of P in the real sample was measured by atomic absorption spectrophotometric (AAS) method. As observed in Fig. 10, removal tests were performed by spiking known amount of standards (30, 150 and 250 mg L^{-1} P ions) in the sample

matrix and then analyzing it. The removal percentage of P from the *Persian Gulf* water reached up to 99.9 and 90.6 and 73.8 % for 30, 150 and 250 mg L^{-1} P, respectively, after 30 min. However, when the adsorbent dosage was increased to 0.5 g adsorption capacity reached up to 99.2 % for 250 mg L^{-1} P after 180 min. The results confirmed that OBW-HNO_3-NZVI has reliable and potent potential to uptake P ions from the real water.

3.7. Mechanism of adsorption

FTIR spectra of OBW-HNO_3-NZVI and P-loaded OBW-HNO_3-NZVI sample, before and after the adsorption process, were recorded in the range of 400 to 4000 cm^{-1} (Figure 11). In the equilibrated sample of the OBW-HNO_3-NZVI with P solution, extra bands at 642 (the bend vibration of O–P–O), 661, 1039 (bending vibration of adsorbed phosphate P-O) and 1056 cm^{-1} (the asymmetric stretch vibration of P–O) appeared confirming the presence of P anchored to the active sites of the immobilized NZVI [42-44]. Furthermore, the peak at 1345 cm^{-1}(O H bending vibration) displayed the existence of hydroxyls groups on the surface of immobilized NZVI, which after removal of P the hydroxyl groups were covered by PO_4^{3-}, and this peak was shifted to 1382 cm^{-1} and weakened [42]. The bands of 414 to 500 cm^{-1} observed in samples were attributed to metal oxygen stretching vibration [45]. The new peaks appeared after phosphate adsorption onto OBW-HNO_3-NZVI, probably showing the presence of inner-sphere surface complex (Fe-O-P) between phosphate and the active sites of NZVI. Also, the kinetics results proved that the adsorption obeyed a pseudo second-order kinetics model that indicated that the adsorption involved physisorption and chemisorptions.

In order to better understand the mechanism and interactions of the phosphate removal from aqueous solution by using OBW-HNO_3-NZVI, XRD pattern of the OBW-HNO_3-NZVI was recorded after shaking with the P solution (Fig. 12), where XRD analysis confirmed that presence of P on OBW-HNO_3-NZVI. The powder XRD pattern was complicated by the presence of iron oxides and oxyhydroxides while showed a progression of reflections associated with $Fe_3(PO_4)_2.8H2O$ (vivianite). Thereby, 2 θ at 13.5° (1), 18.3° (2), 20.21° (3), 22.14° (4), 27.7° (5), 29.5° (6) and 34.0° (8) corresponded to vivianite. However, Fig. 12 shows the immobilized NZVI oxidation after reaction with P, where the apparent reflections at the 2θ of 32.0° (7), 39.5° (9) 43.2 ° (10), 52.4° (13) and 44.9° (11) indicated the presence of magnetite/maghemite (Fe_3O_4/γ-Fe_2O_3) and Fe(0), respectively [46]. Indeed, magnetite (a conductive iron oxide) [47], can give a conductive environment between the reactive surface species in solution and the inner electron-rich core, where the existence of maghemite or hematite at the surface, both less conductive than magnetite could potentially reduce the reactivity and oxidation rate of NZVI. Thus, the peak of Fe(0) could still be found and the peak intensity for Fe(III) and Fe(II) increased, showing that Fe(0) had not been oxidized completely on the surface of OBW-HNO_3-NZVI.

4. Conclusion

The above data demonstrate that the ostrich bone waste is a suitable support for NZVI. The modified bone suppressed the NZVI particles from oxidation and aggregating together even after one year. The adsorption of P ions on OBW-HNO_3-NZVI is well represented by the Langmuir isotherm, whereas kinetics corresponds to a pseudo-second-order equation. XRD analysis showed the appearance of $Fe_3(PO_4)_2.8H2O$ (vivianite) on the OBW-HNO_3-NZVI surface after adsorption of P from aqueous media. The immobilized NZVI indicated high reusability because of its high removal capacity even after 12th adsorption–desorption cycles. The developed adsorbent could also be used to remove the P ions from the real sample (*Persian*

Gulf water). The high removal capacity of P ions from the real water and the high levels of reusability confirmed the versatility of this nanobiomaterial based on ostrich bone waste.

The removal efficiency of the proposed adsorbent with some recently prepared P ions adsorbents are collected in Table 6, where the removal efficiency of OBW-HNO_3-NZVI for P is shown to be higher than that of the majority of other adsorbents considered. Adsorbents having iron active sites in their framework activated a higher P adsorption efficiency. Furthermore, the real water (*Persian Gulf* water) results, display that the heterogenized NZVI on the ostrich bone waste is a promising nanobiomaterial compared to other adsorbents published in the literature for removal of P from the contaminated wastewater. Additionally to the adsorption capacity and being environmentally benign, economic considerations can also determine whether a new system can be used in environmental clean-up solutions or not. Because of cheap, local availability, no need for a costly regeneration system, easy synthesis in large quantities, chemical and thermal stability of the modified ostrich bone waste, OBW-HNO_3-NZVI has an important potential for the sequestration of phosphate ions from the aqueous media.

Acknowledgments

Thanks are due to the Iranian Nanotechnology Initiative for supporting of this work. The authors thank the referees for their valuable comments.

References

[1] D. Cordell, J.O. Drangert, S. White, Global Environ. Change. 2009,19, 292.
[2] V.L. Snoeyink, D. Jenkins, Water Chemistry, Wiley, 1980.
[3] W.J. Eilbeck, G. Mattock, Chemical processes in wastewater treatment, John Wiley, NewYork, 1987.
[4] G. Akay, B. Keskinler, A. Cakici, U. Danis, Water Res. 1998, 32, 717.
[5] Y. Zhao, J. Wang, Z. Luan, X. Peng, Z. Liang, L. Shi, J. Hazard. Mater. 2009, 165, 1193.
[6] W.C. Dennison, R.J. Orth, K.A. Moore, J.C. Stevenson, V. Carter, S. Kollar, P.W.
[7] Bergstrom, R.A. Batiuk, , Bioscience 1993, 43, 86.
[8] U.S. Environmental Protection Agency (USEPA), 1986. Quality Criteria for Water 1986. Office of Water, Regulation and Standard, Washington, DC 20460. EPA 440/5-86-001.
[9] Florida Everglades Forever Act, 1994. Florida State Legislature, Tallahassee, FL.
[10] E. Lacasa, P. Canizares, C. Saez, F.J. Fernandez, M.A. Rodrigo, Chem. Eng. J. 2011, 172, 137.
[11] H.G. Kim, H.N. Jang, H.M. Kim, D.S. Lee, T.H. Chung, Desalination 2010, 250, 629.
[12] E.C. Moreno, K. Varughese, J. Cryst. Growth 1981, 53, 20–30.
[13] L.E. de-Bashan, Y. Bashan, Water Res. 2004, 38, 4222.
[14] I. Katz, C.G. Dosoretz, Desalination 2008, 222, 230.
[15] Zhipan Wen, Yalei Zhang, Chaomeng Dai. Colloids and Surfaces A: Physicochem. Eng. Aspects 2014, 457, 433–440.
[16] Fei Long, Ji-Lai Gong, Guang-Ming Zeng, Long Chen, Xi-Yang Wang, Jiu-Hua Deng,Qiu-Ya Niu, Hui-Ying Zhang, Xiu-Rong Zhang. Chem. Eng. J. 2011, 171, 448.
[17] C. Novillo, D. Guaya, A. Allen-Perkins Avendaño, C. Armijos, J.L. Cortina, I. Cota. Fuel 2014, 138, 72.
[18] J. Jortner, C.N.R. Rao, Pure Appl. Chem. 2002, 74, 1491.
[19] M. Arshadi, F. Salimi Vahid, J. W. L. Salvacion, M. Soleymanzadeh, Appl. Surf. Sci. 2013, 280, 726.
[20] M. Arshadi, F. SalimiVahid, J. W. L. Salvacion, M. Soleymanzadeh, RSC Adv., 2014, 4, 16005.
[21] M. Arshadi, M. Soleymanzadeh, J.W.L. Salvacion, F. SalimiVahid, J. Colloid Interface Sci. 2014, 426, 241.
[22] M. Boroumand Jazi, M. Arshadi, M.J. Amiri, A. Gil, J. Colloid Interface Sci. 2014, 422, 16.
[23] M. Soleymanzadeh, M. Arshadi, J.W.L. Salvacion, F. SalimiVahid,. Chem. Eng. Res. Des. 2015, 93, 696.
[24] M. Arshadi, A.R. Faraji, M.J. Amiri, Chem. Eng. J. 266 (2015) 345–355.
[25] M. Arshadi, Manganese chloride nanoparticles: a practical adsorbent for the sequestration of Hg(II) ions from aqueous solution, Chem. Eng. J. 2015, 259, 170.
[26] R.A. Crane,T.B. Scott, J. Hazard. Mater. 2012, 211– 212, 112.
[27] T. Tosco, M. P. Papini, C. C. Viggi, R. Sethi, J. Clean. Prod., 2014, 77, 10.
[28] Y. Zhou, B. Gao, A. R. Zimmerman, H. Chen, M. Zhang, X. Cao, Bioresour. Technol., 2014, 152, 538.
[29] M.D. Ranganayaki, T.S. Srinivasan. CFTRI, Mysore, 1999, 187.
[30] M. Arshadi, A.R. Faraji, M.J. Amiri, M. Mehravar, A. Gil, J. Colloid Interface Sci. 2015, 446, 11.

[31] D. D. Perrin, W. L. F. Armarego, D. R. Perrin, Purification of Laboratory Chemicals; Pergamon: New York, 1983.
[32] R. Cason, W.R. Lester, Proc. Okla. Acad. Sci. 1977, 57, 116.
[33] F. Peters, K. Schwarz, M. Epple, Thermochim. Acta 2000, 361, 131.
[34] A. Shemesh,. Crystallinity and diagenesis of sedimentary apatites. Geochim. Cosmochim. Ac. 1990, 54, 2433.
[35] T. Ishikawa, M. Wakamura, S. Kondo, Langmuir 1989, 5, 140.
[36] E. T. Stathopoulou, V. Psycharis, G. D. Chryssikos, V. Gionis, G. Theodorou, Palaeogeogr. Palaeoclimatol. Palaeoecol. 2008, 266, 168.
[37] A. T. Tu, in: R.J.H. Clark, R.R. Hester (Eds.), Spectroscopy of Biological Systems, Wiley, New York, 1986, p. 47.
[38] W. Akhtar, H.G.M. Edwards, D.W. Farwell, M. Nutbrown, Spectrochim. Acta A 1997, 53, 1021.
[39] X.-Y. Wang, Y. Zuo, D. Huang, X.-D.Hou, Y.-B. Li, Biom. Environ. Sci. 2010, 23, 473.
[40] T. Almeelbi, A. Bezbaruah, J. Nanopart. Res., 2012, 14, 900.
[41] Z. Wen, Y. Zhang, C. Dai, Colloids and Surfaces A: Physicochem. Eng. Aspects 2014, 457, 433.
[42] H. Li, J. Ru, W. Yin, X. Liu, J. Wang, W. Zhang, J. Hazard. Mater. 2009, 168, 326.
[43] D.S. Soejoko, M.O. Tjia, J. Mater. Sci. 2003, 38, 2087.
[44] H.L. Liu, X.F. Sun, C.Q. Yin, C. Hu, J. Hazard. Mater. 2008, 151, 616-622.
[45] S.K. Apte, S.D. Naik, R.S. Sonawane, B.B. Kale, J. Am. Ceram. Soc. 2007, 90, 412.
[46] . Kim, H., Hong, H.J., Lee, Y.J., Shin, H.J., Yang, J.W. Desalination 2008, 223, 212.
[47] R. M. Cornell, U.Schwertmann, The Iron Oxides: Structure, Properties, Reactions, Occurrences and Uses, 2 ed.; Wiley-VCH: Weinheim, Germany, 2003; pp 129, 235, 506-508, 537-538, 506-508.
[48] S. Hamoudi, R. Saad, K. Belkacemi, Ind. Eng. Chem. Res. 2007, 46, 8806.
[49] V.K. Gupta, A. Mittal, L. Kurup, J. Mittal, J. Colloid Interface Sci. 2006, 304, 52.
[50] P. Ning, H.J. Bart, B. Li, X. Lu, Y. Zhang, J. Environ. Sci. 2008, 20, 670.
[51] Asim Olgun, Necip Atar, Shaobin Wang, Chemical Engineering Journal 2013, 222, 108.
[52] B.K. Biswas, K. Inoue, K.N. Ghimire, H. Harada, K. Ohto, H. Kawakita, Bioresour. Technol. 2008, 99, 8685.
[53] X. Huang, X. Liao, B. Shi, J. Hazard. Mater. 2009, 166, 1261.
[54] K.A. Krishnan, A. Haridas, J. Hazard. Mater. 2008, 152, 527.
[55] M.R. Unnithan, V.P. Vinod, T.S. Anirudhan, J. Appl. Polym. Sci. 2001, 84, 2541.
[56] T.L. Eberhardt, S.H. Min, Bioresour. Technol. 2008, 99, 626.
[57] Weiya Huang, Yi Zhu, Jinpeng Tang, Xiang Yu, Xuelei Wang, Dan Li and Yuanming Zhang. J. Mater. Chem. A, 2014, 2, 8839.
[58] J. Antelo, S. Fiol, C. Perez, S. Marino, F. Arce, D. Gondar, R. Lopez, J. Colloid Interface Sci. 2010, 347, 112.
[59] C. Liu, Y. Li, Z. Luan, Z. Chen, Z. Zhang, Z. Jia,. Adsorption removal of phosphate from aqueous solution by active red mud. J. Environ. Sci. 2007, 19, 1166.
[60] K. Barthélémy, S. Naille, C. Despas, C. Ruby, M. Mallet. J. Colloid Interface Sci. 2012, 384, 121.
[61] Adva Zach-Maor, Raphael Semiat, Hilla Shemer, J. Colloid Interface Sci. 2011, 357, 440.

[62] T.S. Anirudhan, P. Senan, Chem. Ecol. 2011, 27, 147.

Table captions

Table 1. Results of chemical analysis of the prepared biomaterials.

Table 2. The physicochemical properties of the bone samples.

Table 3. Kinetic parameters for the adsorption of P ions by OBW-HNO_3-NZVI at different initial concentrations.

Table 4. Thermodynamic parameters for the adsorption of P ions on OBW-HNO_3-NZVI as a function of temperature.

Table 5. Fitting of the parameters of the experimental results to the Langmuir and Freundlich equation parameters.

Table 6. Comparison of P ion adsorption capacities at different adsorbents.

Table 1. Results of chemical analysis of the prepared biomaterials.

Chemical analysis wt.%*	C	N	S	Al	Na	P	K	Mg	Ca	Mn	Fe
Pristine ostrich bone	79.8	4.21	1.78	1.92	2.39	2.35	0.92	2.01	2.18	1.36	1.08
OBW-HNO_3	18.5	8.69	2.8	2.66	3.5	20.3	2.7	3.0	33.1	2.2	2.6
OBW-HNO_3-NZVI	5.12	2.21	0.41	4.87	2.45	28.9	1.6	2.76	39.2	3.2	9.2

*Carbon, nitrogen and sulfur were estimated from the elemental analysis (CHN). The other elements were determined from ICP analysis.

Table 2.The physicochemical properties of the bone samples.

	Pristine ostrich bone	OBW-HNO_3	OBW-HNO_3-NZVI
Total surface area (m^2/g)	3.7	18.42	41.4
Average pore size[a](Å)	43	69.48	75.6

[a] The pore size calculated using the BJH method.

709

Table 3. Kinetic parameters for the adsorption of P ions by OBW-HNO_3-NZVI at different initial concentrations.

C_o (mg L^{-1})	$q_{e,exp}$ (mg g^{-1})	Pseudo first order			Pseudo second order				Intra-particle diffusion	
		k_1 (min^{-1})	q_1 (mg g^{-1})	R^2	k_2 (g (mg min)$^{-1}$)	q_2 (mg g^{-1})	h (mg (g min)$^{-1}$)	R^2	K_{int} (mg (g $min^{1/2})^{-1}$)	R^2
30	29.4	0.408	100	0.4465	0.208	29.76	185.1	0.9952	3.906	0.4507
70	65.0	0.533	181.8	0.5635	0.173	69.4	834	0.9948	9.529	0.4902
250	191	0.556	500	0.5817	0.001	192.3	1428	0.9951	26.00	0.4443

710

711

712

Table 4. Thermodynamic parameters for the adsorption of P ions on OBW-HNO_3-NZVI as a function of temperature.

Initial P conc. mg L^{-1}	$-\Delta H^o$ (J mol^{-1})	ΔS^o (J (mol K) $^{-1}$)	$-\Delta G^o$ (kJ·mol^{-1})			
			258	298	333	353
70	88.31	315.0	81.36	93.96	104.9	111.3
250	40.56	144.4	37.30	43.08	48.13	51.02
800	2.916	5.574	1.441	1.664	1.859	1.970
1000	2.842	3.230	0.836	0.965	1.078	1.143

713

714

715

716

Table 5. Fitting of the parameters of the experimental results to the Langmuir and Freundlich equation parameters.

	q_m	K_L	K_F	n	R^2	Sorption model
OBW-HNO_3-NZVI						
	1679	1.93×10^{-3}			0.9870	Langmuir
			0.470	0.285	0.957	Freundlich
OBW-HNO_3						
	20.3	1.86×10^{-2}			0.9590	Langmuir
			3.60×10^{-2}	1.28	0.3891	Freundlich
Pristine ostrich bone						
	3.93	3.73×10^{-2}			0.9740	Langmuir
			1.30×10^{-2}	2.33	0.4410	Freundlich

717

718

719

Table 6. Comparison of P ion adsorption capacities at different adsorbents.

Adsorbent	q_{max} (mg g^{-1})	Ref.
NZVI	245.6	[15]
Corn stalk based resin	40.48	[48]
Lanthanum-doped activated carbon fiber (ACF-La)	9.41	[49]
Activated alumina	53.7	[50]
boron waste (BW)	52.5	[51]
Zr(IV) loaded orange waste gels	175	[52]
Fe(III) loaded skin split waste	72	[53]
Fe(III) impregnated coir pith	70.92	[54]
Fe(III) loaded carboxylated polyacrylamide grafted sawdust	28.79	[55]
Wood modified by carboxymethyl cellulose/$FeCl_2$	17.38	[56]
HMS-1/5	47.9	[57]
Ferrihydrite	83.5	[58]
Acid activated red mud	202.9	[59]
Ferric green rust $Fe^{III}_6 O_4(OH)_8CO_3 . 3H_2O$	64.8	[61]
Nano-iron oxide-impregnated granular activated carbon (nFe-GAC)	435	[61]
Fe(III)-AM-PGMACell	77.2	[62]
OBW-HNO_3-NZVI	326	This work

720

721

Figure captions

Figure 1. FTIR spectra of the ostrich bone waste (A), OBW-HNO_3 (B) and OBW-HNO_3-NZVI (C).

Figure 2. TEM micrographs of ostrich bone waste (A) and OBW-HNO_3-NZVI (B).

Figure 3. X-ray diffraction patterns of the unmodified and modified ostrich bone by HNO_3 and NZVI.

Figure 4. (A) Effect of the pH on P adsorption by OBW-HNO_3-NZVI from aqueous solutions and (B) zeta potential of the modified bone samples as a function of pH ($C_{Bone\ samples}$ = 2.5 g dm^{-3} and 10^{-3} mol dm^{-3} solutions of KNO_3). Experimental error: ±4 mV.

Figure 5. The adsorption kinetics (A) and effect of initial concentrations (B) for the adsorption of P on the OBW-HNO_3-NZVI at 25ºC.

Figure 6. (A) The Vant Hoff's plot for determination of thermodynamic parameters of P on the OBW-HNO_3-NZVI and (B) equilibrium absorption of P by the modified bone samples at 25 ◦C and pH = 5.0.

Figure 7. The effect of chloride, nitrate, bicarbonate, sulfate and citrate on the removal of P by OBW-HNO_3-NZVI; pH = 5.0, C_0 = 250 mgL^{-1}, contact time = 24 h, T = 25 ^oC.

Figure 8. The effect of concentration of NaOH on the desorption of P from OBW-HNO_3-NZVI (A), and adsorption capacity of OBW-HNO_3-NZVI after repeated regeneration (B).

Figure 9. Values of the percentage removal of P ions at different initial concentration on OBW-HNO_3-NZVI samples kept for various aging times before being used as adsorbents.

Figure 10. P removal from the *Persian Gulf* water after exposure to OBW-HNO_3-NZVI at varying times.

Figure 11. FTIR spectra of OBW-HNO_3-NZVI before (A) and after (B) adsorption of P from aqueous solution (P = 250 mg L^{-1}, OBW-HNO_3-NZVI = 0.05 g).

Figure 12. Wide-range X-ray diffraction of OBW-HNO_3-NZVI-P (P = 250 mg L^{-1}, OBW-HNO_3-NZVI = 0.05 g).

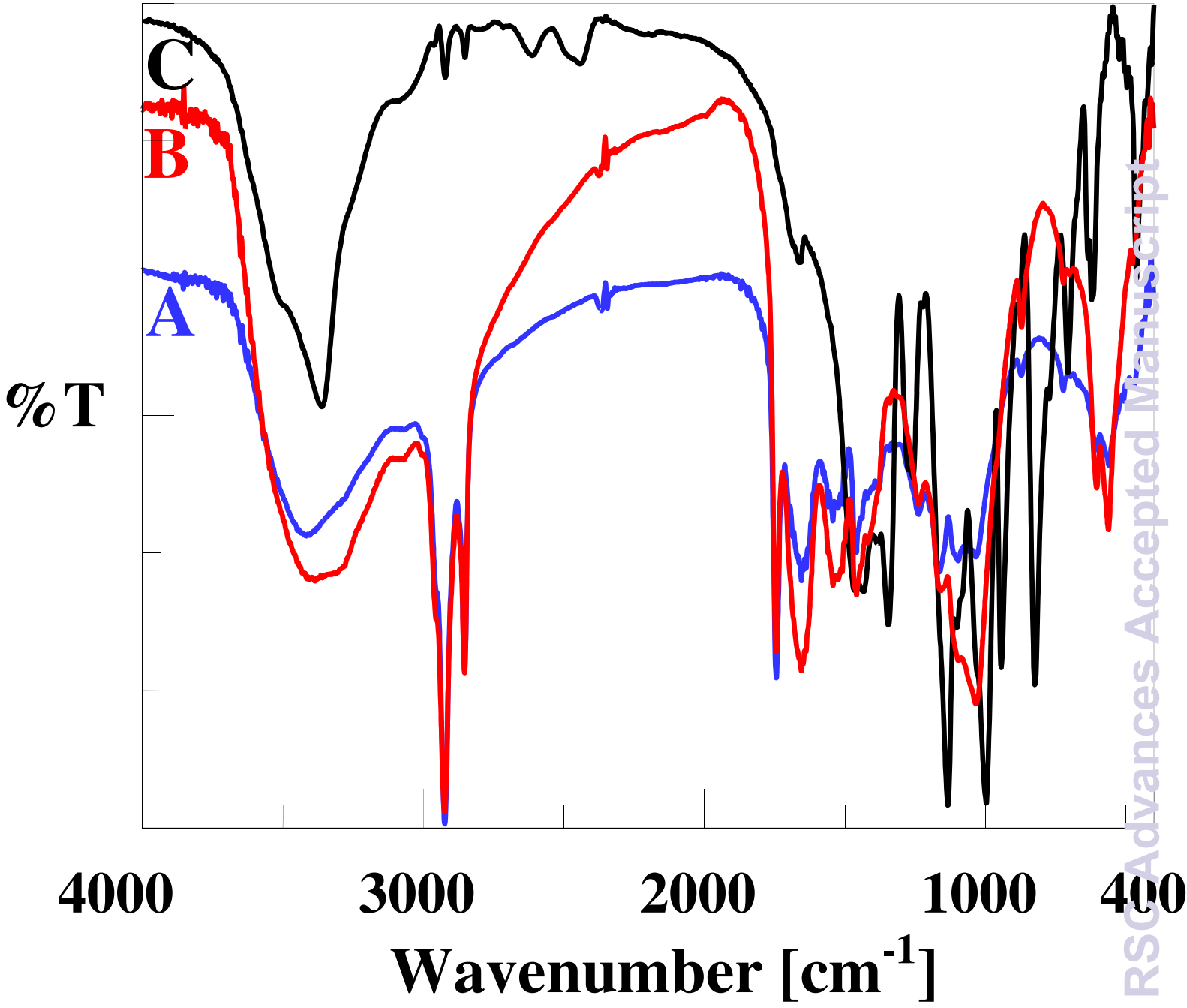

Figure 1. FTIR spectra of the ostrich bone waste (A), OBW-HNO_3 (B) and OBW-HNO_3-NZVI (C).

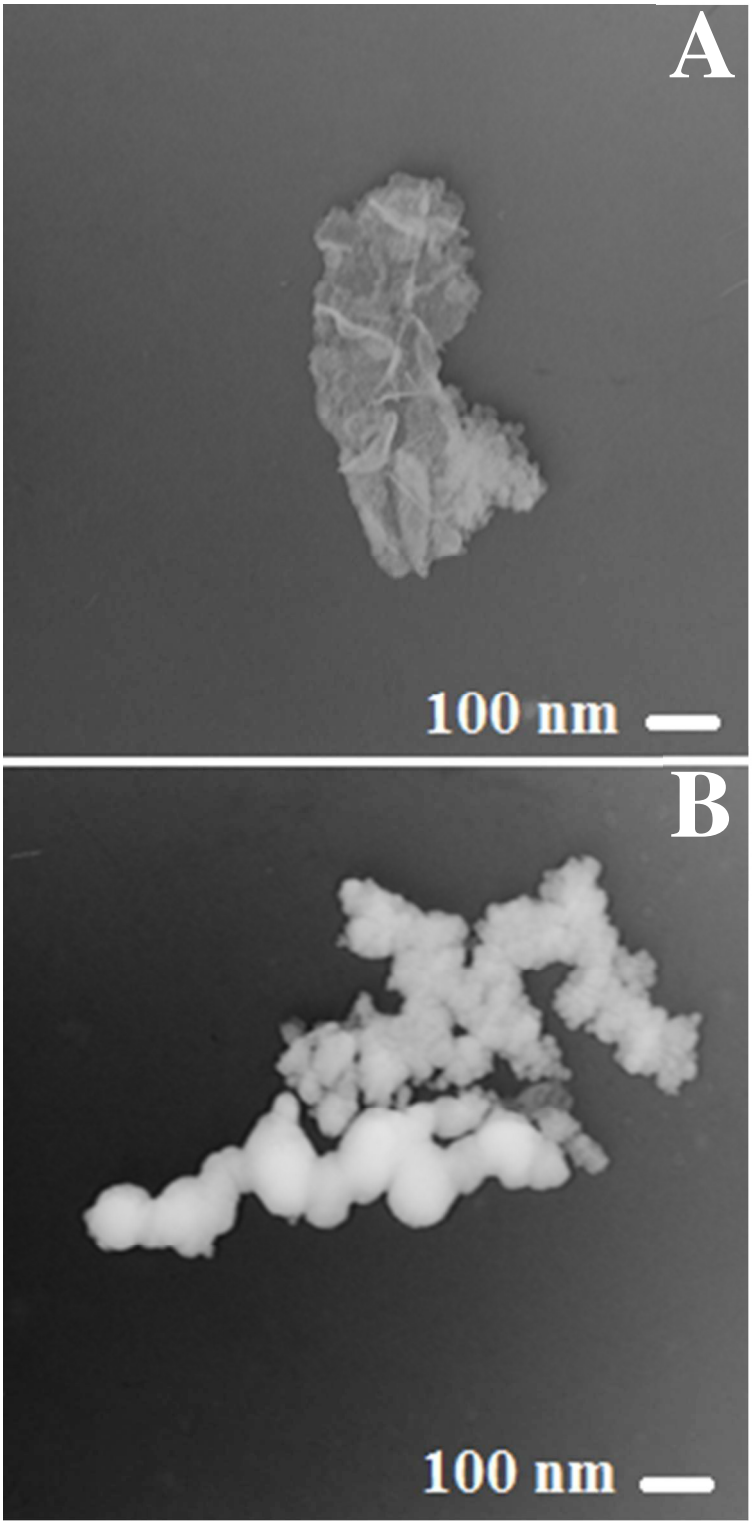

Figure 2. TEM micrographs of ostrich bone waste (A) and OBW-HNO_3-NZVI (B).

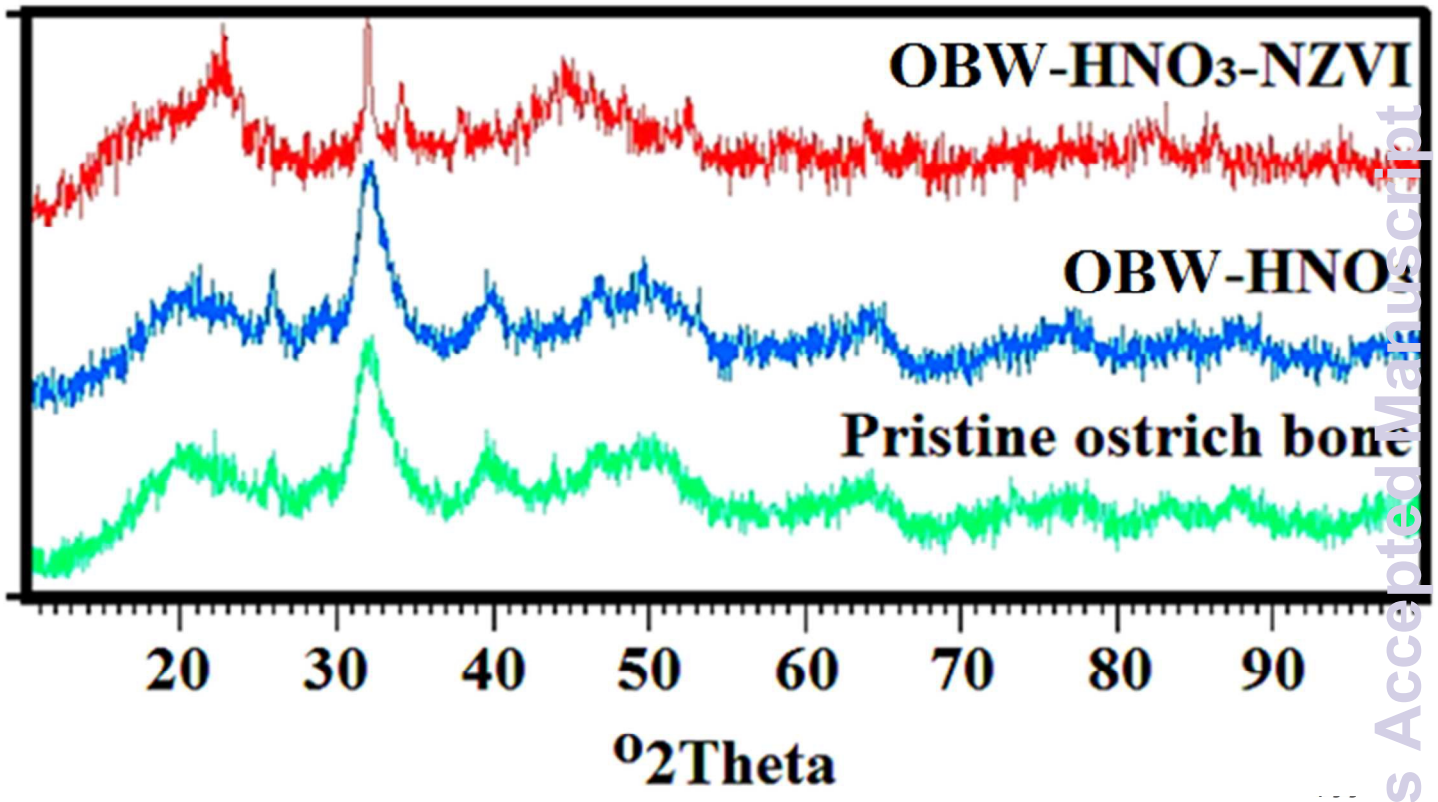

Figure 3. X-ray diffraction patterns of the unmodified and modified ostrich bone by HNO_3 and NZVI.

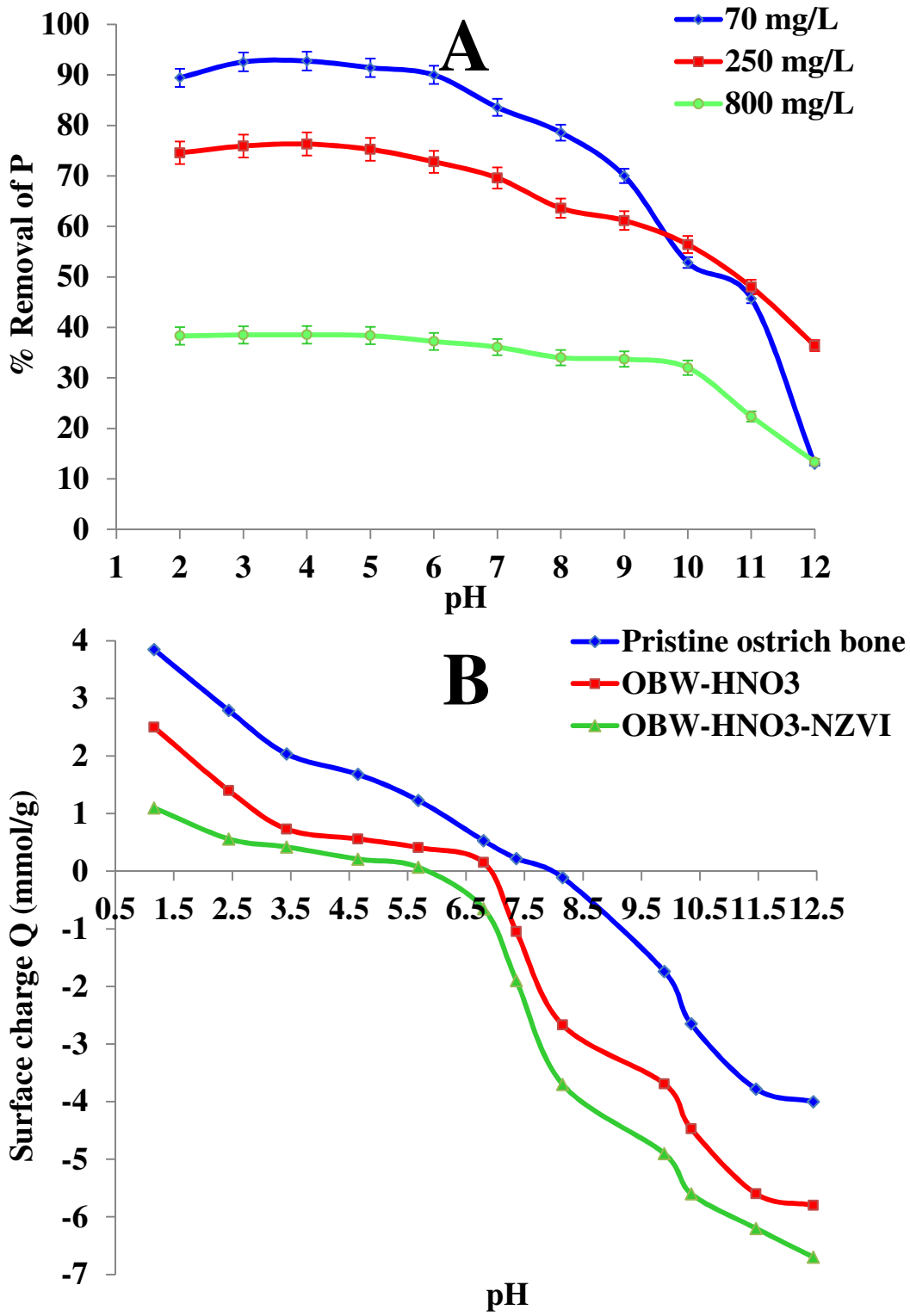

Figure 4. (A) Effect of the pH on P adsorption by OBW-HNO_3-NZVI from aqueous solutions and (B) zeta potential of the modified bone samples as a function of pH ($C_{Bone\ samples}$ = 2.5 g dm^{-3} and 10^{-3} mol dm^{-3} solutions of KNO_3). Experimental error: ±4 mV.

768

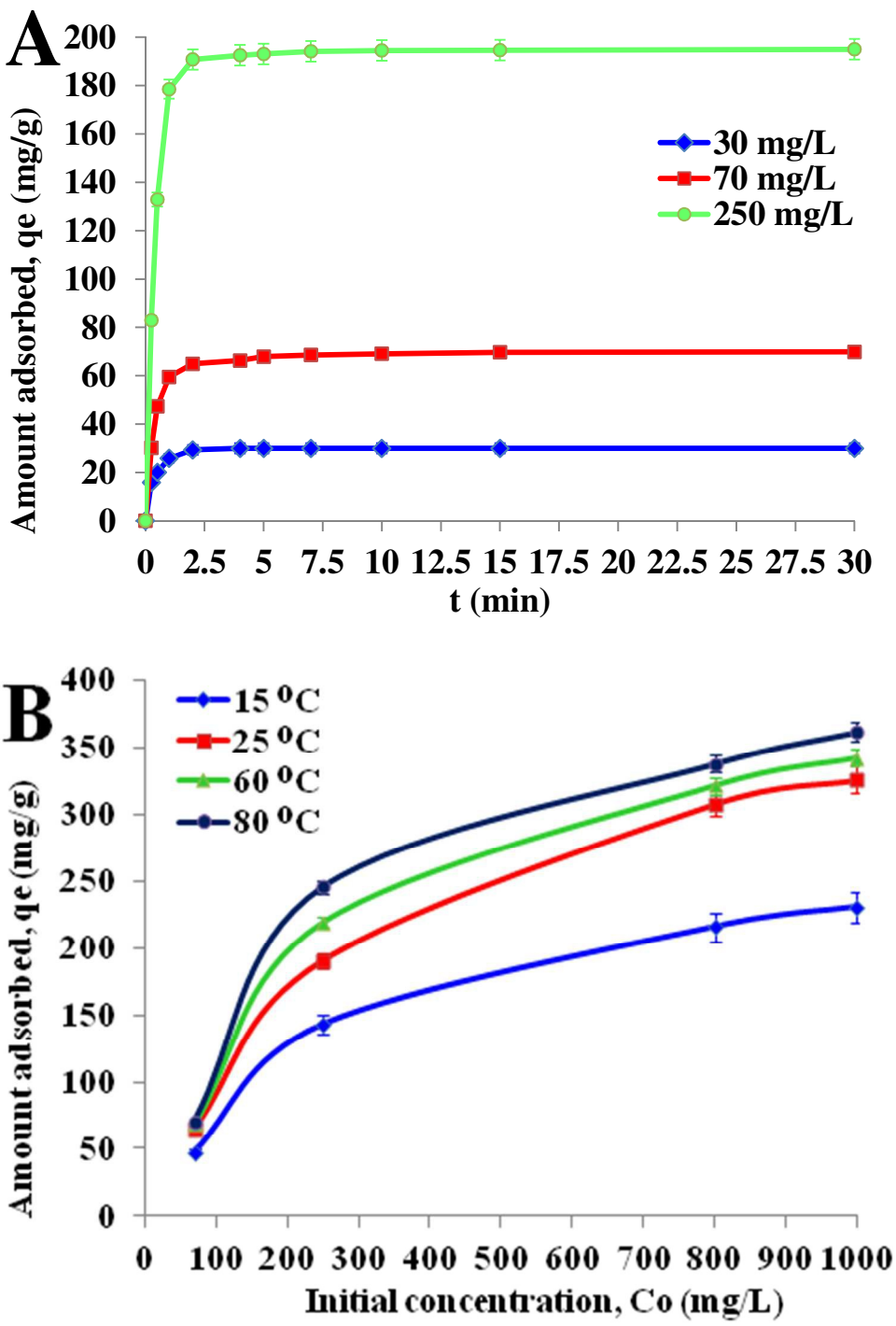

Figure 5. The adsorption kinetics (A) and effect of initial concentrations (B) for the adsorption of P on the OBW-HNO_3-NZVI at 25ºC.

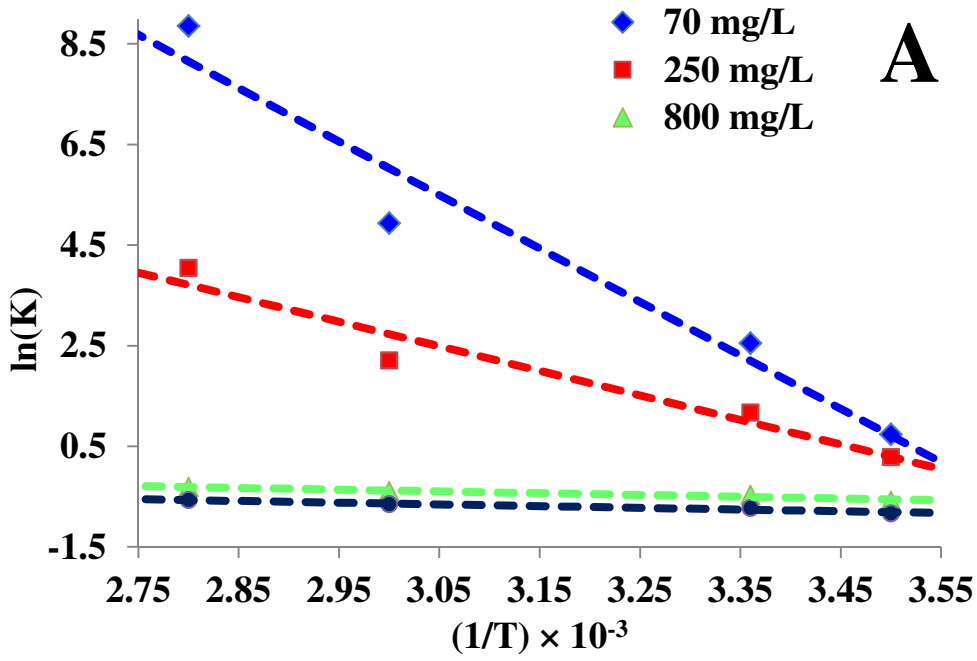

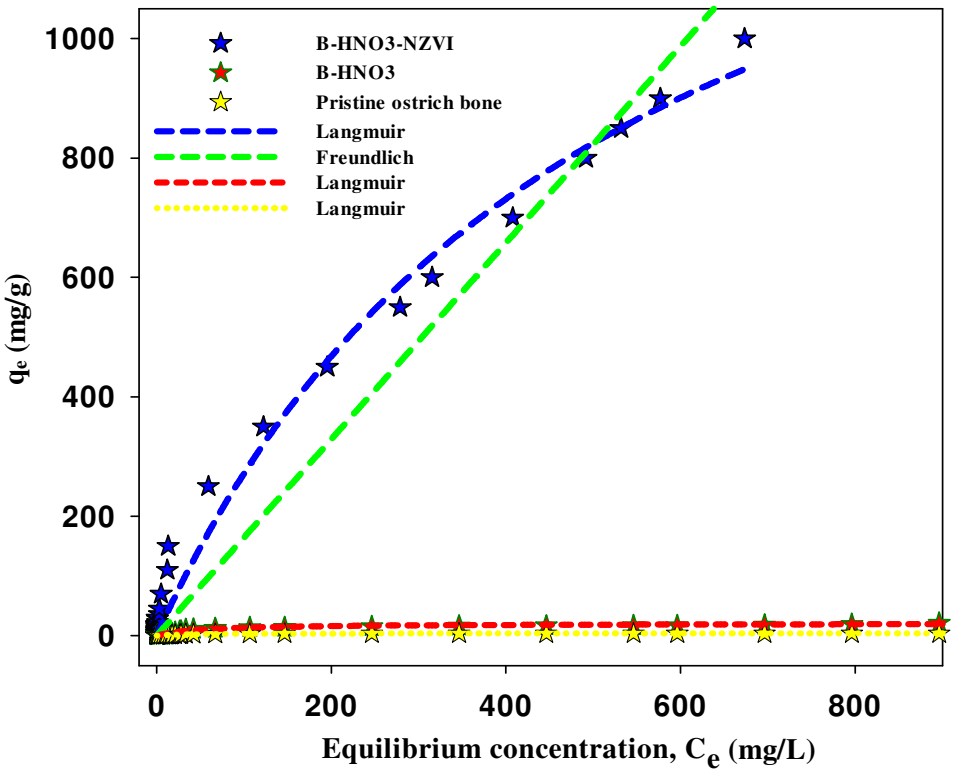

Figure 6. (A) the Vant Hoff's plot for determination of thermodynamic parameters of P on the OBW-HNO_3-NZVI and (B) equilibrium absorption of P by the modified bone samples at 25 ◦C and pH = 5.0.

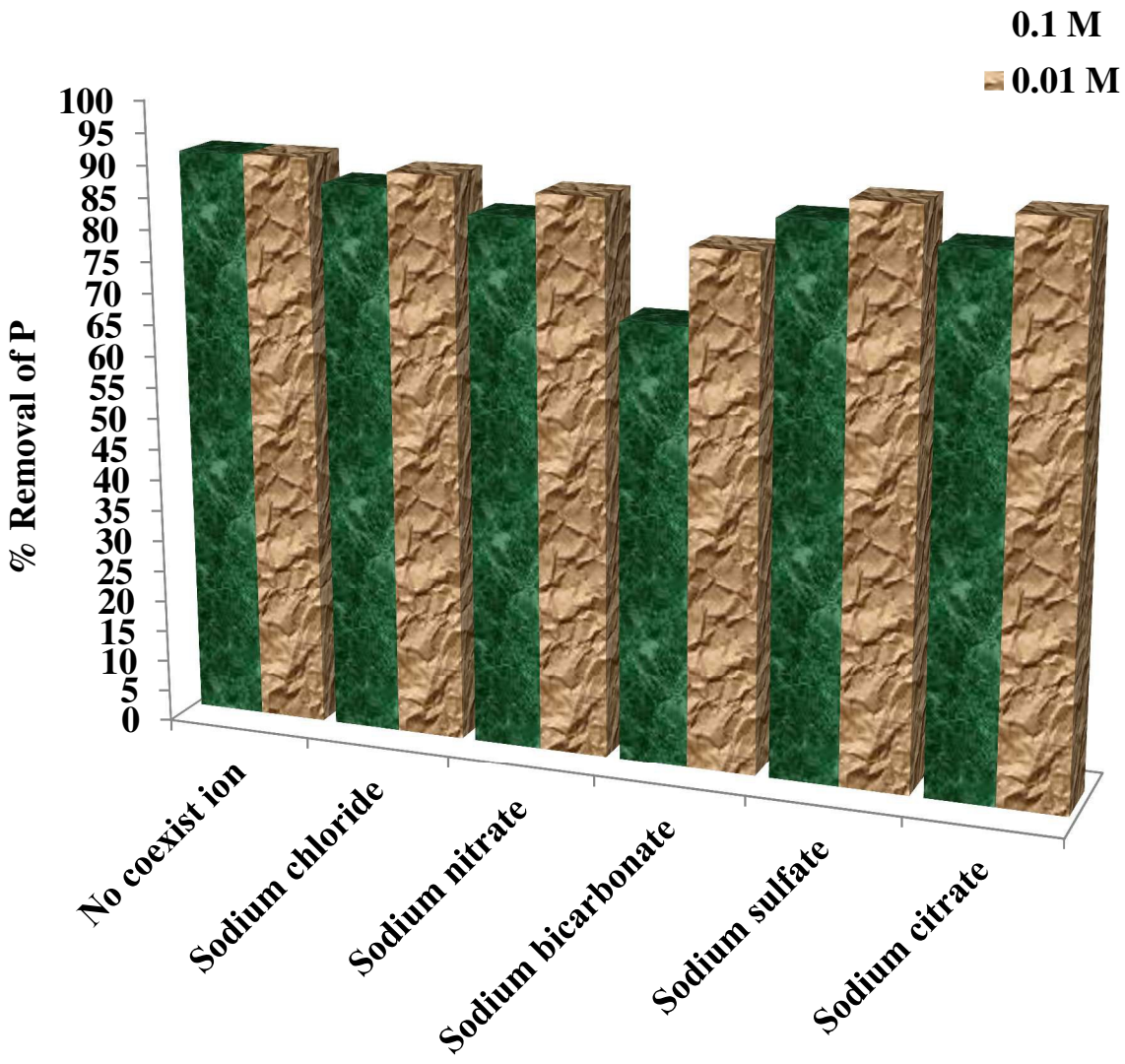

Figure 7. The effect of chloride, nitrate, bicarbonate, sulfate and citrate on the removal of P by OBW-HNO_3-NZVI; pH = 5.0, C_0 = 500 mg L^{-1}, contact time = 24 h, T = 25 ^oC.

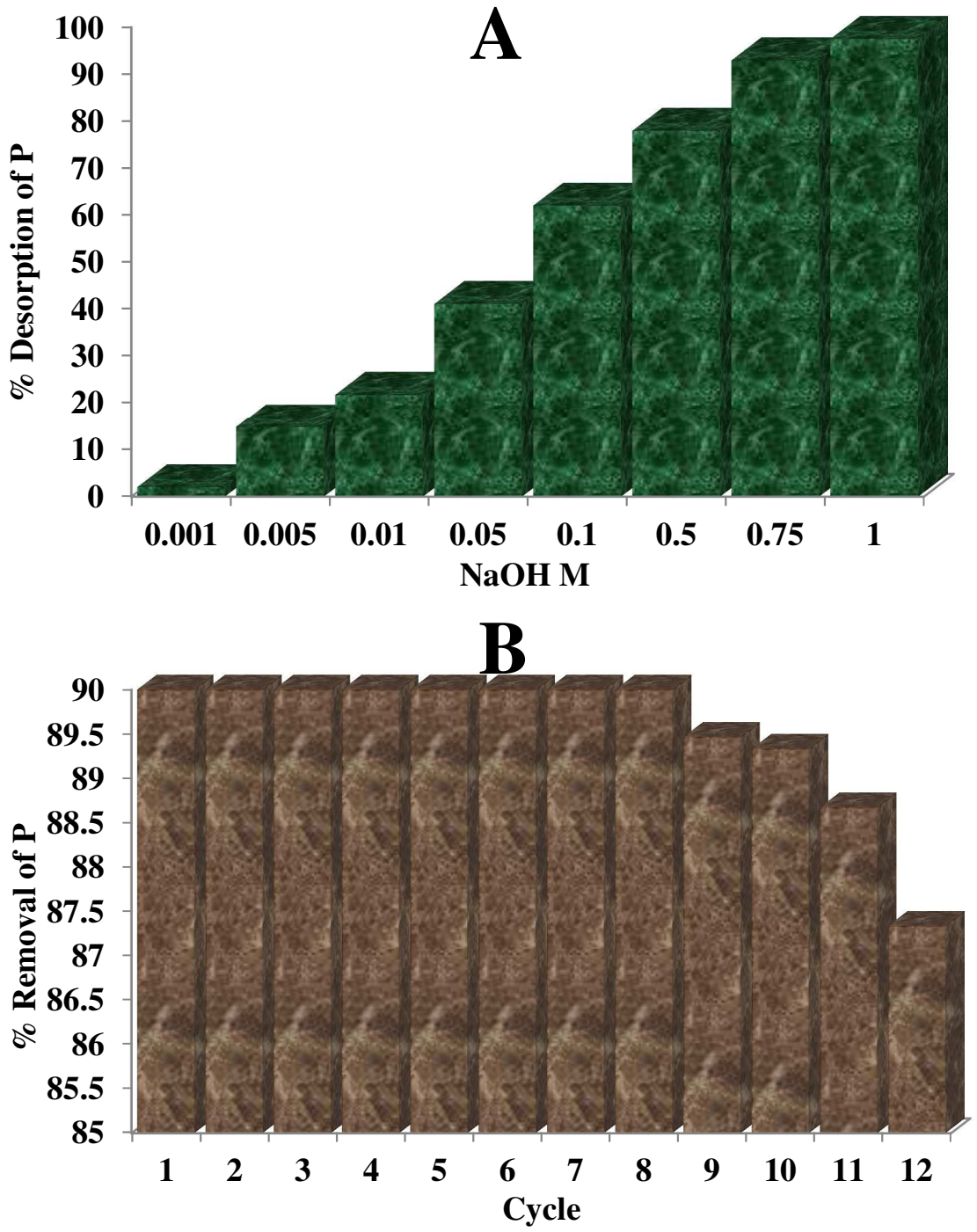

Figure 8. The effect of concentration of NaOH on the desorption of P from OBW-HNO_3-NZVI (A), and adsorption capacity of OBW-HNO_3-NZVI after repeated regeneration (B).

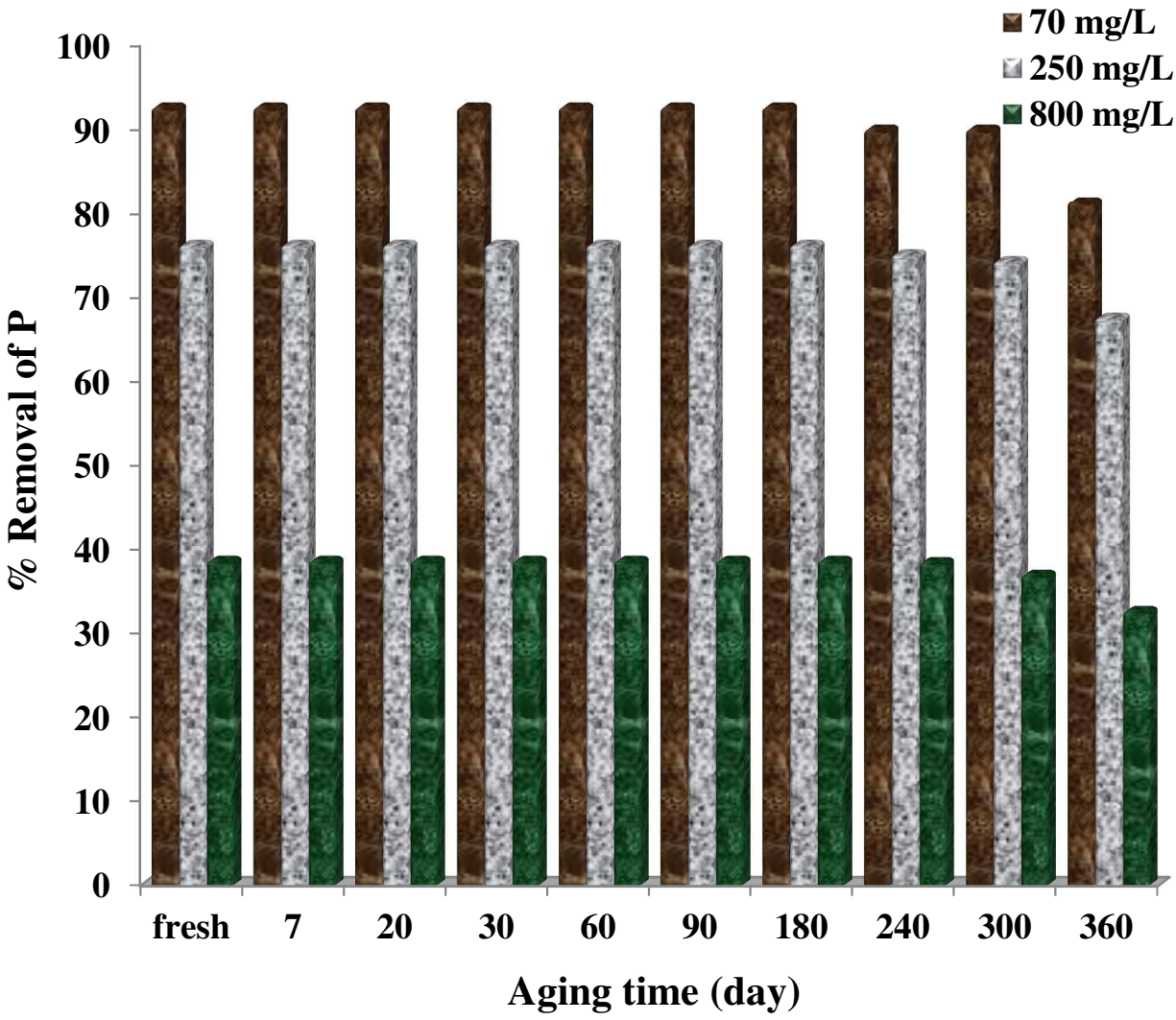

Figure 9. Values of the percentage removal of P ions at different initial concentration on OBW-HNO_3-NZVI samples kept for various aging times before being used as the adsorbent.

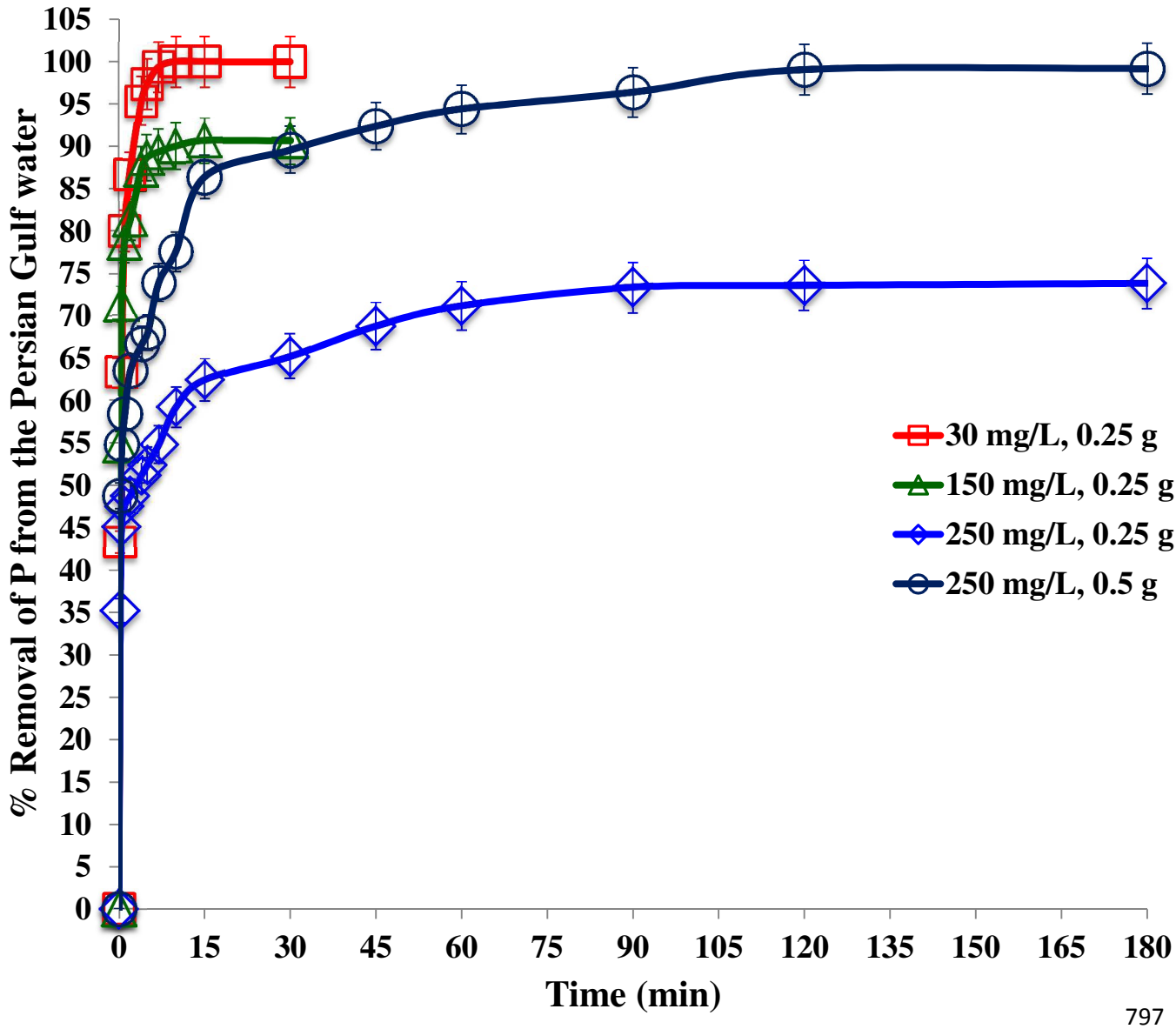

Figure 10. P removal from the *Persian Gulf* water after exposure to OBW-HNO_3-NZVI at varying times.

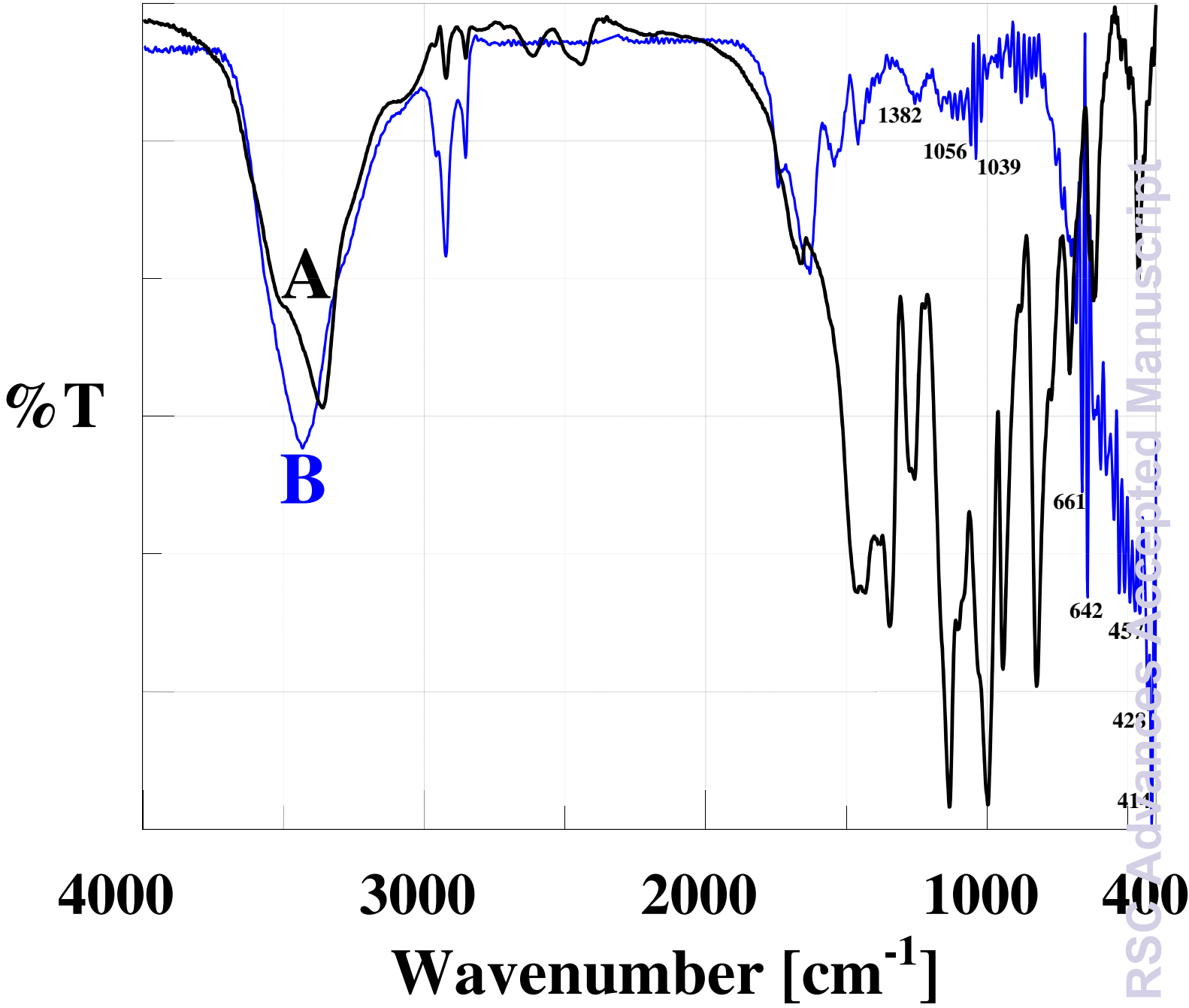

Figure 11. FTIR spectra of OBW-HNO_3-NZVI before (A) and after (B) adsorption of P from aqueous solution (P = 250 mg L^{-1}, OBW-HNO_3-NZVI = 0.05 g).

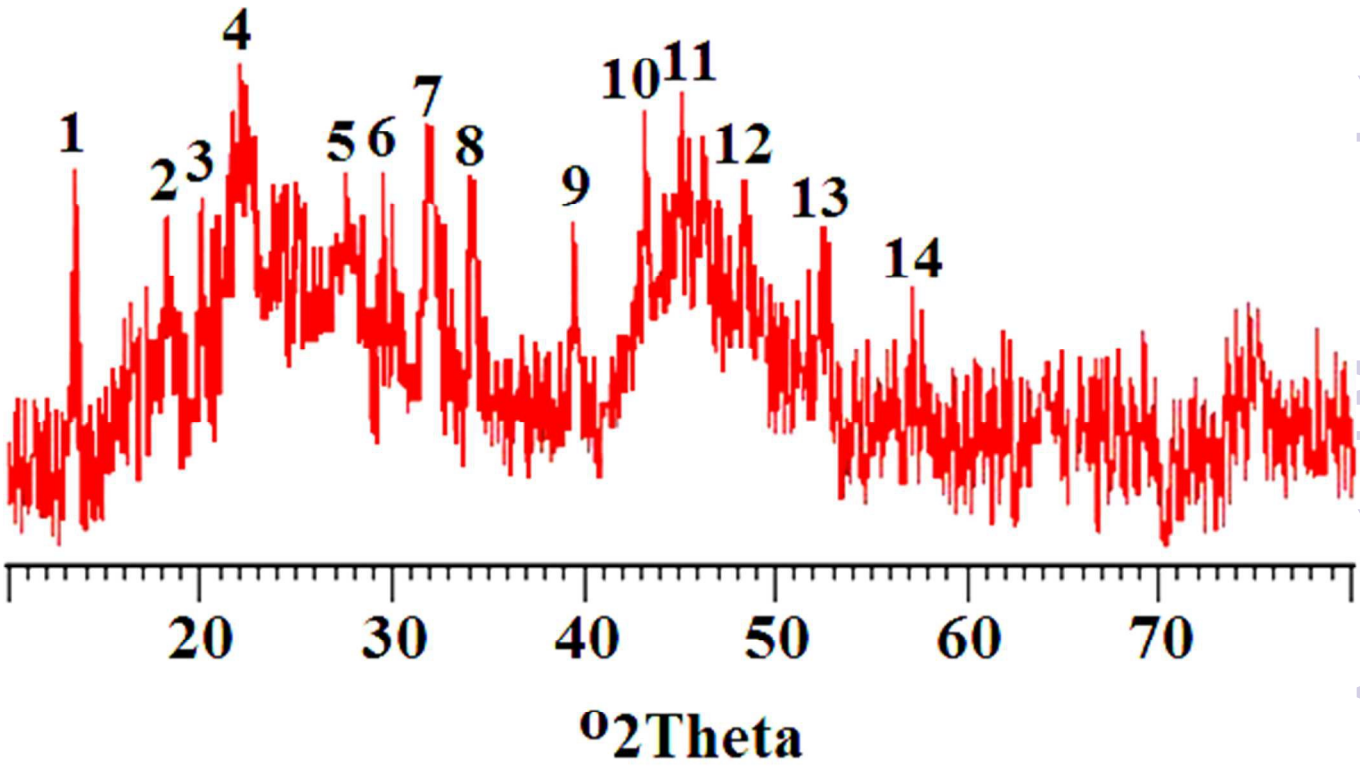

Figure 12. Wide-range X-ray diffraction of OBW-HNO_3-NZVI-P (P = 250 mg L^{-1}, OBW-HNO_3-NZVI = 0.05 g).